

# Surface Modification of 6xxx Series Aluminum Alloys

Kuruveri Udaya Bhat <sup>1,\*</sup>, Devadas Bhat Panemangalore <sup>1</sup>, Spandana Bhat Kuruveri <sup>2</sup>, Merbin John <sup>3</sup>  
and Pradeep L. Menezes <sup>3,\*</sup>

<sup>1</sup> Department of Metallurgical and Materials Engineering, National Institute of Technology, Mangalore 575025, Karnataka, India; devadasbhatp@gmail.com

<sup>2</sup> Department of Mechanical Engineering, National Institute of Technology, Mangalore 575025, Karnataka, India; spandbhat@gmail.com

<sup>3</sup> Department of Mechanical Engineering, University of Nevada, Reno, NV 89557, USA; merbinjohn@nevada.unr.edu

\* Correspondence: udayabhatk@nitk.edu.in (U.B.K.); pmenezes@unr.edu (P.L.M.)

**Abstract:** Due to their superior mechanical properties, formability, corrosion resistance, and lightweight nature, 6xxx series aluminum (Al) alloys are considered as a promising structural material. Nevertheless, the successful application of these materials depends on their response to the external environment. Recently, designers considered the surface properties an equally important aspect of the component design. Due to this concern, these alloys are subjected to varieties of surface modification methodologies. Many methodologies are explored to modify the 6xxx series Al alloys surfaces effectively. These methods are anodizing, plasma electrolytic oxidation (PEO), cladding, friction stir processing, friction surfacing, melting, alloying, and resolidification using high energy beams, etc. This review work discusses some of these methods, recent research activities on them, important process variables, and their role on the final properties of the surfaces.

**Keywords:** surface modification; aluminum alloys; microstructure; anodizing; plasma electrolytic oxidation; laser cladding; friction surfacing



**Citation:** Bhat, K.U.; Panemangalore, D.B.; Kuruveri, S.B.; John, M.; Menezes, P.L. Surface Modification of 6xxx Series Aluminum Alloys. *Coatings* **2022**, *12*, 180. <https://doi.org/10.3390/coatings12020180>

Academic Editors: Ioannis Karapanagiotis and Elvira De Giglio

Received: 6 January 2022

Accepted: 26 January 2022

Published: 30 January 2022

**Publisher's Note:** MDPI stays neutral with regard to jurisdictional claims in published maps and institutional affiliations.



**Copyright:** © 2022 by the authors. Licensee MDPI, Basel, Switzerland. This article is an open access article distributed under the terms and conditions of the Creative Commons Attribution (CC BY) license (<https://creativecommons.org/licenses/by/4.0/>).

## 1. Introduction

The need for weight reduction and improvement in mechanical properties in automobile, aerospace, sports, and health care industries has stimulated the development of new materials and processes. In addition, the requirement of material with specific functional properties has also contributed to the growth of this particular domain [1–6]. Aluminum (Al) alloys and their derivatives form an important sector in this development. However, the actual deployment of these materials and their components also depends on their response to the environment, in addition to their microstructural and mechanical properties [7–10]. Hence, in a majority of the alloy applications, altering the surface behavior is considered an equally important goal in materials development [11].

Al is available in plenty in the earth's crust. Unfortunately, pure Al is highly soft and ductile, hence, unusable for structural applications. For structural and other load-bearing applications, Al is alloyed with various alloying elements so that the resultant alloy will have desired mechanical, chemical, and physical properties, such as strength, stiffness, toughness, corrosion resistance, and physical appearance [12]. Based on the added alloying elements, alloys are classified into various groups, namely 2xxx, 3xxx, 4xxx, 5xxx, 6xxx, etc. Mechanical properties of the Al alloys could be altered with thermal, mechanical, or thermo-mechanical treatments. Most of the 6xxx series Al alloys are used in T4 or T6 temper conditions. T4 indicates that the alloy is solution treated and is naturally aged to a stable state without the support of the cold work. T6 implies that the alloy is solution heat-treated, and without any cold work, it is artificially aged to achieve precipitation hardening [13]. The following section illustrates the predominantly used Al 6000 series alloys, their mechanical properties, alloying elements, and intended applications.

### 1.1. 6xxx Grade Al Alloys

6xxx series Al alloys consist of silicon (Si) and magnesium (Mg) as the primary alloying elements, with Al as the host element. These alloys have good strength and ductility, enhanced corrosion resistance, ease of formability, and anodizability [7]. Additionally, they have good weldability, which makes them a strong candidate for structural applications. Mg and Si are added in a ratio required to form quasi-binary alloy (Al-Mg<sub>2</sub>Si) alloys with (Mg:Si:: 1.73:1) or with an excess of Si than required for the equilibrium magnesium silicide (Mg<sub>2</sub>Si) formation. The formation of Mg<sub>2</sub>Si facilitates the scope for heat treatment and improvement in strength [3,14,15].

#### 1.1.1. Alloy 6005A

This alloy is considered a structural alloy with medium strength. It probably has the lowest quantity of alloying elements in 6xxx series Al alloys, which are of practical relevance. Moreover, this alloy has good bending properties. It is used in tubing form for various profiles for furniture used in buses and railways.

#### 1.1.2. Alloy 6061

The 6061 alloy is precipitation-hardenable, and it has good corrosion resistance. Because of these features, it has found applications in designing aircraft frames [16]. Since the Al 6061 alloy is a common and reliable alloy for structural applications, it is called “structural Al”. It is a first-choice material where higher strength and structural support are required. It is used for building small multipurpose naval vessels, aircraft components, such as fuselage and wings, bicycle frames, motorcycles, etc. Mechanical properties, such as yield strength (YS), ultimate tensile strength (UTS), shear strength, and fatigue strength, could be varied by using various processing or tempering. The 6061 alloys are extensively used under T6 conditions, solutionizing followed by precipitation hardening [17,18]. It has a number of intermetallic compounds, namely, CuAl<sub>2</sub>, Mg<sub>2</sub>Si, MgZn<sub>2</sub>, etc., driving precipitation strengthening [19].

#### 1.1.3. Alloy 6063

This grade is most commonly used for extrusion. It could be extruded into thin-walled, small, and intricate shapes and, hence, is used extensively for structural applications. For such applications, invariably, T6 temper is used. AA6063 grade is generally considered as an extrusion grade; hence, plates and rolled variants are generally not available. This grade has good corrosion resistance and average machinability characteristics. AA6063 alloy is used extensively in buildings. Anodic oxidation could be used to produce a surface with beautiful colors and hence extensively used in architectural applications. It is used to manufacture furniture, vessels, motor vehicles, window frames, door frames, roof support systems, etc. Compared to 6061, 6063, it is more corrosion resistant and exposed to more severe environments. Alloy 6063 with T6 tempering has average bending and folding characteristics. Alloy 6063 tubes and bars of T6 temper can be bent reasonably, but that is not a guaranteed feature. Compared to T6 temper, T4 temper has higher cold working and formability characteristics.

#### 1.1.4. Alloy 6082

It is another Al grade with commercial purity. It has the highest strength amongst various 6xxx grade alloys with proper heat treatment, making it suitable for structural applications involving welding and machining. It is used in various forms: sheets, plates, bars (square and round), channels, and angles. It is generally used under T6 conditions. It can be used even in outdoor applications. Grade 6082-T6 is amenable for polishing and powder coating. Table 1 illustrates the mechanical properties of the important 6xxx series Al alloys [20].

**Table 1.** Chemical composition and basic mechanical properties of important 6xxx series Al alloys. YS, UTS, and Elongation in 50 mm gauge.

Alloy Type and Temper	Composition (wt%)	Mechanical Properties
6005A-T6	Si: 0.6–0.9, Fe: 0.3–0.6, Cu: $\leq$ 0.1, Mn: $\leq$ 0.1, Mg: 0.4–0.6, Cr: $\leq$ 0.01, Zn $\leq$ 0.1, Ti $\leq$ 0.1 Al: balance	YS: 200 MPa, UTS: 250 MPa, Elong: 8%
6061-T6	Si: 0.4–0.8, Fe: $\leq$ 0.7, Cu: 0.15–0.4, Mn: $\leq$ 0.15, Mg: 0.8–1.2, Cr: 0.04–0.35, Zn $\leq$ 0.25, Ti $\leq$ 0.15 Al: balance	YS: 276 MPa, UTS: 310 MPa, Elong: 12%
6063-T6	Si: 0.2–0.6, Fe: $\leq$ 0.35, Cu: $\leq$ 0.1, Mn: $\leq$ 0.1, Mg: 0.45–0.9, Cr: $\leq$ 0.10, Zn $\leq$ 0.15, Ti $\leq$ 0.1 Al: balance	YS: 214 MPa, UTS: 241 MPa, Elong: 12%
6082-T6	Si: 0.7–1.3, Fe: $\leq$ 0.5, Cu: $\leq$ 0.1, Mn: $\leq$ 0.4–1.0, Mg: 0.6–1.2, Cr: $\leq$ 0.25, Zn $\leq$ 0.2, Ti $\leq$ 0.1 Al: balance	YS: 260 MPa, UTS: 310 MPa, Elong: 10%

## 2. Need for Surface Modification of 6xxx Series Al Alloys

Many high-strength 6xxx series Al alloys are developed based on physical metallurgy and materials design concepts. Many of these alloys are susceptible to degradations initiated at the surface. For example, intermetallic compounds in the 6xxx series alloys make them susceptible to corrosion forms, such as pitting and stress-assisted corrosion [21,22]. The Federal Aviation Administrative Advisory (FAAA) circular on corrosion control identifies the following three corrosions experienced by the high strength Al alloys. They are:

- (i) pitting corrosion;
- (ii) stress corrosion cracking;
- (iii) intergranular corrosion.

Protective coatings are used to protect Al alloys from corrosive environments [6]. Basically, such coatings isolate structural members from the environments, improving the material's corrosion resistance. Some of these coatings are developed following hard anodizing, cladding, priming, cold spraying, plasma electrolytic oxidation (PEO), and similar methods [23–26]. When they are put into service, some of the Al alloys would be experiencing mechanical and tribological conditions. For such situations, surface modification technologies, such as rapid solidification, using laser and electron beam remelting, friction stir processing, and friction surfacing are employed [27,28]. The following sections deal with these methodologies with reference to 6xxx series Al alloys as the substrate material.

## 3. Anodizing

Anodizing is one of the oldest, traditional electrochemical processes of Al finishing in the metal industry. In general, anodizing is the process by which the surface of the Al or its alloys is converted to porous Al oxide. By enhancing the thickness of the naturally protective Al oxide on the surface (which is typically 5–25 nm), one can develop a high-performance finish with a range of colors that is corrosion-resistant, non-toxic, durable, paintable, abrasion-resistant, aesthetic in appearance, low-cost, and non-hazardous. Anodizing is an electrochemical conversion process. Here, the part that will be surface modified is made the anode in an electrolytic cell. The electrolyte could be of various types: chromic acid, sulfuric acid, borate or tartrate baths, phosphoric acids, and organic acids such as malic acid, oxalic acid, etc. The cell would be operated under DC voltages that may run-up to a few tens of volts. A pre-treatment, such as electrolytic/abrasive polishing that will influence the coating's properties, would be performed before anodizing. The developed porous surface can accept dyes, and one can impart a range of colors onto the finished products. Based on the final applications, two distinct types of anodizing are carried out. They are soft anodizing and hard anodizing. Hard anodizing is applied for heavy (or experiencing wear conditions) industrial parts that are exposed to aggressive

and corrosive environments. They are thicker and harder, which helps in increasing their durability. The anodized layer can cover the surface irregularities.

In contrast, the soft anodizing process produces a surface layer that is optically transparent. Most of the mechanical properties remain the same, and they are mainly used for decorative applications. The difference between these processes is the operating temperature, use of additives, current density, and applied voltage. Being a group of Al-based alloys, 6xxx series Al alloys have good anodizability. From an anodizing perspective, the 6060 Al alloy is explored much more compared to other types of 6xxx series alloys. Alloy 6060 is a treatable heat alloy offering moderate strength but better extrudability. It has good corrosion resistance and weldability and is used for complex cross-sections. Polat et al. [29] used the Taguchi method to design an optimum anodic polarization process for 6060 alloys. Four parameters, such as additive type, dissolved Al concentration, bath temperature, and current densities, were used to prepare an L9 orthogonal array. As a result, the anodized samples exhibited a varied range of corrosion current densities and potentials that reflect their changes with respect to characteristics of the anodized film, namely the pore size and its distribution, geometry, and structure of the anodized film.

Wilson et al. [30] studied anodizing of 6060 Al alloy using sulfuric acid as the electrolyte by a method called sulfuric acid anodizing (SAA). They explored the effect of the tartaric acid addition on the anodization of AA6060-T6 alloy, focusing on improving corrosion resistance and adhesiveness with the post painting layer. Tartaric-sulfuric acid anodizing (TSA) was studied further to improve the corrosion resistance of the anodic film. Since the same anodizing line was used for SAA and TSA, it was essential to assess the commercial feasibility and cross-contamination. It was found that contamination in the tanks was unlikely as they were rinsed with distilled water, and it did not affect the adhesive bond strength values. Knudsen et al. [31] explored anodizing as a pre-treatment prior to organic coating of EN AW-6060 (T6). Both alternating current (AC) hot anodizing (80 °C) and direct current (DC) anodizing (20 °C) were performed as pre-treatment. Hot AC anodizing developed 0.1–0.5 µm oxide thickness when the sample was treated in 15 wt.% of H<sub>2</sub>SO<sub>4</sub> electrolytes for 5 s. It performed better than DC anodizing due to its surface cleaning effect. This process also removes Fe-rich intermetallics and decreases the cathodic current density, thereby enhancing filiform corrosion resistance property. This process is environmentally friendly as the chemicals used do not contain chromium and is robust due to better voltage-current control. Tabrizian et al. [32] have conducted anodizing a 6060 Al alloy to study optical properties. They tailored anodizing of 6060 alloys by opting for cold-forging, heat-treatment, and diamond turning operations. They observed that prior deformation increases anodized layer thickness. Heat-treatment levels offset the effect of prior deformation. This is shown by the power spectral density measurements that produced lower scattering. Due to post-forging heat treatment, the distribution of intermetallic particles such as Si and Mg<sub>2</sub>Si improved. These dispersed particles and defects in the oxide film also contributed to lower brightness values for the anodized film measured using the bidirectional reflection distribution function.

Short and Bryant reviewed defects appearing on anodizing Al [33]. Ma et al. [34] studied the streak formation during anodizing of AA6063-T6 extruded alloy. Pre-etching of the alloy followed by anodizing is associated with the formation of grain boundary streaks. Etching steps and surface scallops are affecting the streaking regions during anodization. In turn, grain size distribution and crystallographic orientation could affect the streaking regions. Extruded AA6063 exhibited a strong texture, and it could affect the anodization by promoting streaking regions and non-uniform anodization.

Bononi et al. [35] have explored the effect of current amplitude and frequency on the anodizing of AA6082-T6 alloy, focusing on volumetric expansion ratio, anodic oxide thickness, and hardness of the samples. A comparison with AA2024-T3 and AA7075-T6 showed the influence of precipitates and composition on the anodizing treatment. The 6xxx series exhibited a relatively better tendency to become anodized. Higher frequency caused an increase in the thickness, but it reduced the compactness of the anodized layer.

Hardness remained almost constant. Aggerbeck et al. [36] studied the optical appearance of an anodized layer on AA6082. It is found that with an increased degree of alloying, the second phase particles led to increased roughness of the as-etched surface, which is indicated by the diffuse reflections in the bidirectional reflectance distribution function. Wielage et al. [37] investigated the effect of pre-treatment of the substrate's surface on the thickness of the anodized films on EN AW-6082-T6 alloys. The film thickness was measured using an atomic force microscope and surface profilometer. As-received samples exhibited greater surface roughness. With the increase in coating thickness, as-received samples also exhibited a more significant increase in the roughness values. Grober et al. [38] performed hard anodizing on EN AW-6082 alloys to study the effect of anodizing on fatigue properties for self-tapping screw applications. Although hard anodizing did not vary the static tensile strength, it significantly reduced the fatigue performance of the specimens with respect to the unmodified variants.

#### 4. Plasma Electrolytic Oxidation (PEO)

Plasma electrolytic oxidation (PEO) is a surface treatment method used for obtaining oxide coatings on metals, such as Al, Mg, and titanium. The coating obtained has excellent properties, such as high corrosion resistance, wear resistance, and electrical insulation. These coating properties help them to be used in applications such as medical, aerospace, automotive, oil, and gas industries [39–41]. PEO is an anodic oxidation process. During the PEO process, the alloy to be oxidized is the anode. A shrouding environment of oxygen is ensured around the anode throughout the oxidation process. A high voltage is applied between the anode and the second electrode, usually in the range of tens of voltage to hundreds of volts. The applied voltage is sufficiently high to ensure continuous sparks across the electrolytic environment, separating the anode and the second electrode. The voltage exceeds the dielectric breakdown potential for the growing oxide film. Generally, stainless steel container is used to hold the electrolyte, and it also serves as the second electrode. The pictorial representation of PEO is represented in Figure 1. Sparks and associated chemical reactions ensure a ceramic oxide coating that is less porous on the anode surface. As a result, the coating will have high adhesion to the substrate [42].

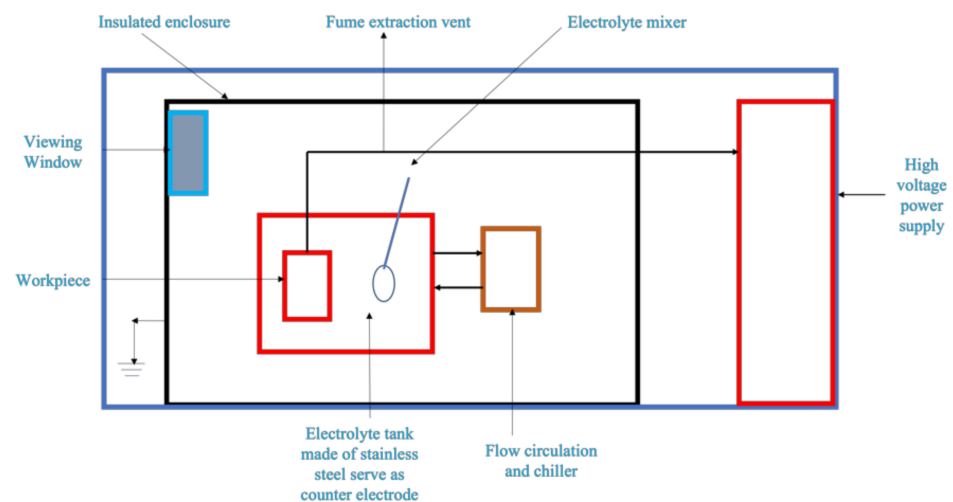


**Figure 1.** Schematic presentation of the system used for the PEO process.

The PEO variables control the properties of the PEO-treated surfaces. Some of them are dielectric medium or electrolyte composition and their concentration, electrical parameters during oxidation, oxidation time, added additives, and their concentration and temperature during oxidation [42–44]. In recent times, PEO treated surfaces have been popular due to the convenience of the process and characteristics of the coatings obtained.

The performance parameters, such as hardness and wear resistance of PEO coatings, are influenced by the coating thickness, phase compositions, size, and amount of pores and microcracks [45]. Some of the characteristics of the PEO coatings could be improved by the incorporation of second phase particles, such as corrosion inhibitors, graphite, graphene, carbon nanotubes (CNT), or by an overlay of epoxy coatings [46–49]. Some of the advantages of PEO coatings are excellent adhesion to the substrate, even with complex geometry. Growth rates are reasonably higher, and the possibility of adding species or modifying the composition of the coatings always opens new application domains [46,50–52]. Under certain deposition conditions, the coatings could be porous. This could be exploited for the benefit of impregnating with the appropriate chemicals. This could help the designer to introduce different functional properties to the surface, namely hydrophobicity, self-lubrication, etc. [49,53]. The type of electrolyte decides some of the limitations of the PEO process. For example, aqueous-based electrolytes are generally associated with a low coating rate, a porous coating, electrolyte need to be cooled to make it a stable electrolyte, encapsulation of undesirable compounds in the coatings, etc. The use of molten salts reduces these limitations [42,54]. This also explains why most of the work on the PEO was conducted using alkali salts. Another limitation could be the expensiveness of the equipment, and the electrolytes are supplied as proprietary.

PEO has many synonyms. Some of them are micro-arc discharge oxidation (MDO), anodic-spark deposition (ASD), micro-arc oxidation (MAO), micro-plasma oxidation (MPO). Technology-wise, it is the derivative of conventional anodizing. However, PEO uses much higher cell voltage and can produce a thicker coating, with very high adhesion to the substrate [55,56]. In general, a PEO coating consists of three layers deposited one above another on the substrate (Refer Figure 2), which is generally a light metal or an alloy. The PEO coating has a comparatively higher porosity than anodizing, but it can efficiently protect the substrate against corrosion. In addition, molten oxides can heal the pores formed by discharge due to high local temperature in the plasma discharge channels.

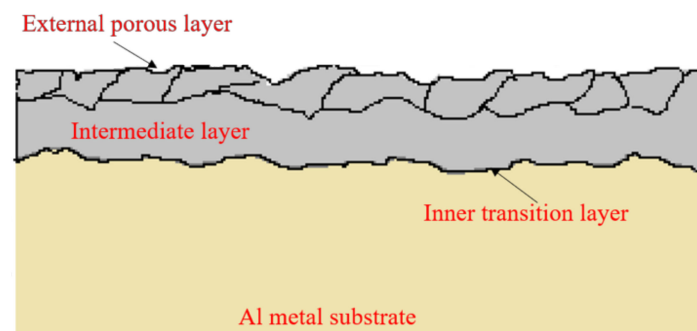


**Figure 2.** Schematic of a cross-sectional micrograph of PEO coating on the Al substrate.

PEO is a relatively new technique, and it is being explored to modify the surfaces of 6xxx series Al alloys for improving wear resistance, microhardness, corrosion resistance, self-lubrication behavior. In the 6xxx series Al alloys domain, the authors could not find any investigation on 6005A alloy and limited research on 6063 and 6082 Al alloys. However, many research articles are available for 6061 Al alloy compared to them. The following section briefly explains the salient features of various 6xxx series Al alloys.

#### 4.1. PEO of 6061 Al Alloys

Various researchers have explored the utility of PEO for improving specific functional properties of the 6061 Al alloy. Zhu et al. [45] revealed improved microhardness and frictional resistance using PEO coatings on the 6061 Al alloy. Their electrolyte was silicate-based, and they used sodium hexametaphosphate as an additive to produce a thick, less porous, and harder PEO coating on 6061 alloys. Their research indicates that sodium hexametaphosphate can alter the microhardness, morphology, and thickness of the PEO

coatings. Sharma et al. [43] used KOH containing  $\text{Na}_2\text{SiO}_3$  as the electrolyte. They used various ratios of KOH and  $\text{Na}_2\text{SiO}_3$  to explore the effect of concentration on the PEO oxide layer grown on the 6061 Al alloy, its morphology, and properties. They noted that a higher fraction of  $\text{Na}_2\text{SiO}_3$  produces a hard coating and increases the growth rate. They observed that the coating with optimum properties could be obtained with KOH:  $\text{Na}_2\text{SiO}_3$  equals to 3:2. Wang et al. [44] used an alkaline electrolyte containing NaOH,  $\text{Na}_2\text{SiO}_3$ , and NaCl for the PEO of 6061 Al alloy. They used hybrid voltage conditions and noted that increased values of DC voltages led to increased growth of the ceramic layer. The ceramic layer had a double-layer structure consisting of a hard outer layer and a soft inner layer. Many research investigations focus on improving the functional properties of 6061 by using the PEO process. These properties could improve corrosion resistance, wear, friction, wettability behavior, etc. Dzhurinskiy et al. [6] have used the PEO process for improving the corrosion resistance behavior of 6061-O alloy. The authors used an electrolyte consisting of KOH in  $\text{Na}_2\text{SiO}_3$ . They observed improved corrosion resistance compared to the bare substrate. They could evaluate the coating formation stage distinctly. They also correlated the process parameters, thickness, and corrosion resistance of the PEO coating. Tran [57] explored the possibility of an electrolyte that is alkali-free. They explored an electrolyte containing calcium phosphate and ammonia water for PEO of 6061 Al alloy. They noted that PEO coating has improved hardness and corrosion resistance. Chen et al. [58] used PEO as a process tool to protect the weldment involving dissimilar materials combination of 6061 and 7075 Al alloys. They noted that the PEO oxide coverage on the weldment has different morphology and composition compared to PEO coating on the substrate materials. They also noted that the PEO coating of the weldment reduces the potential difference between various parts and is hence expected to have improved corrosion resistance.

Trevino et al. [59] investigated the effect of the PEO process on the wear resistance of 6061 Al alloy. They produced coatings with thicknesses in the range of 100–150  $\mu\text{m}$  using an electrolyte of KOH and  $\text{Na}_2\text{SiO}_3$  with a voltage in the range of 400–600 V. Figure 3 represents the scanning electron microscopic (SEM) images of the PEO coatings on the oxide coating had phases, such as mullite,  $\alpha$ -alumina,  $\gamma$ -alumina, and amorphous alumina, due to which the coating was much harder than the substrate. The wear studies indicated that the predominant wear modes are adhesion and abrasion. Peng et al. [60] used two different types of electrolytes for PEO of 6061 Al alloy. The electrolytes were KOH + sodium phosphate and KOH + sodium aluminate mixtures. pH value was close to each other in both cases. They observed that the electrolyte with aluminate generated  $\alpha$ -alumina rich single-layered coatings and exhibited better wear resistance than the phosphate-based coatings. PEO coating using phosphate-based electrolyte produced bilayer coatings. The top surface was porous and less dense. The inner layer was rich in phosphorous, and it was a dense layer. Therefore, it exhibited improved corrosion resistance compared to the aluminate-based one.

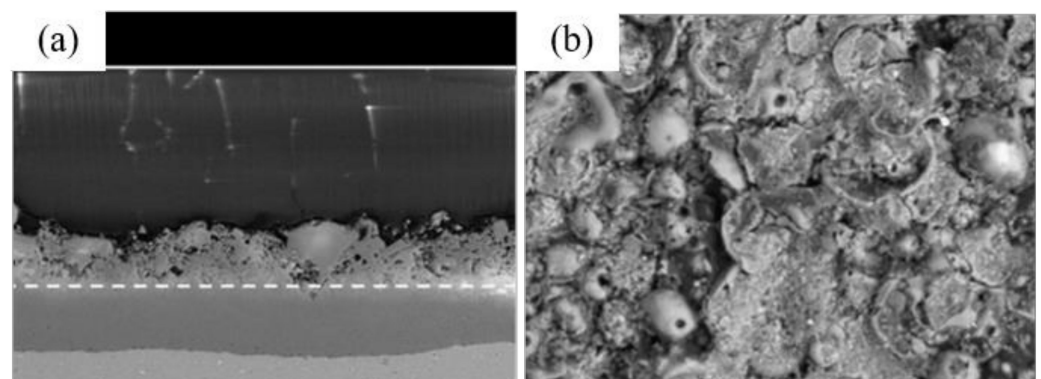


**Figure 3.** SEM of the PEO coatings on 6061 Al alloy (a) cross-section and (b) surface using KOH+  $\text{Na}_2\text{SiO}_3$  electrolyte. Reproduced with permission from [59]. Copyright Elsevier, 2012.

Many researchers used various additives to improve different functional properties of the PEO coatings generated on the surface of the 6061 Al alloy. Sowa et al. [46] added organic corrosion inhibitors to the PEO coatings developed on 6061 Al alloy. They reported that 8-hydroxyquinoline in ethanol could fill the pores produced during the direct current (DC) PEO process, and it exhibited improved corrosion resistance in the NaCl solution medium. Figure 4 presents the surface structure of the PEO coating wherein pores are filled with hydroxyquinoline. The profilometer measurements indicate a noticeable reduction in roughness, which is attributed to the filling of the pores with the 8-hydroxyquinoline. They also noted that thinner the coating, lesser the porosity, and sealing would be better [46]. Tran et al. [61] added diamond powders into the electrolyte containing  $\text{Na}_2\text{SiO}_3$  and  $\text{H}_3\text{BO}_3$ . Their results indicated that adding diamond powders improves coating characteristics, namely thickness, wear, and corrosion resistance. Diamond powders of the level 6g/liter in the electrolyte produced a coating with the optimum properties. It had the best corrosion resistance, microhardness, and lowest friction coefficient. Ma et al. [47] prepared a composite coating using the PEO of 6061 alloys with graphite particles to alkali sodium silicate electrolyte. They noted that the resultant coating has low friction and wear resistance than the bare oxide coatings.

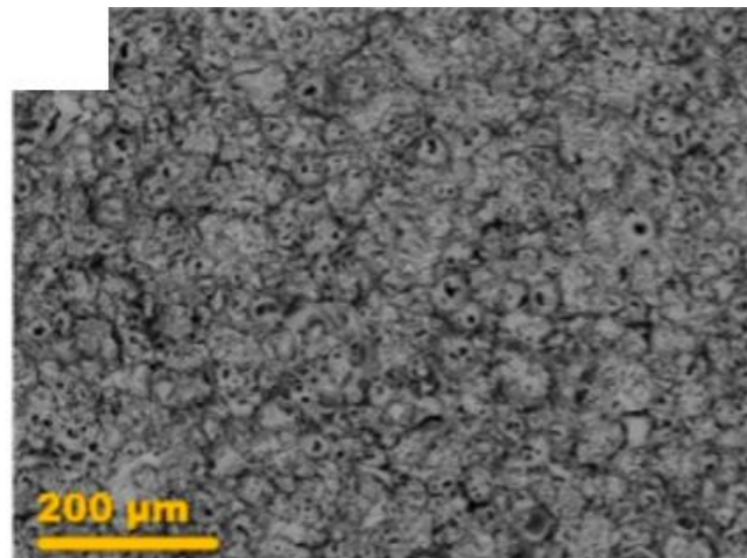


**Figure 4.** Planar view of the PEO oxide films formed on 6061 Al alloy under the processing conditions of  $440 \text{ mA/cm}^2$  + 8-hydroxyquinoline + DC supply. Reproduced with permission from [46].

Byeon et al. [62] have conducted the PEO of the AA6061 alloy. They introduced N during PEO to enhance hardness and anti-abrasion properties. The Oxynitride layer was developed using a combination of electrolytes, such as  $\text{NaNO}_3$ ,  $\text{NaAlO}_2$ , and  $\text{NaOH}$ . The surface morphology of coatings comprised of pan-like microstructures, and the phase composition was made of AlON,  $\alpha\text{-Al}_2\text{O}_3$ , and  $\gamma\text{-Al}_2\text{O}_3$ . The  $\text{NO}_3^-$  ions in the electrolyte reacted with  $\gamma\text{-Al}_2\text{O}_3$  to form the AlON phase. Madhavi et al. [63] explored the effect of pre-shot peening on the PEO of AA6061-T6 specimens and the influence of surface roughness on the corrosion fatigue life of PEO-oxide-coated 6061-T6 specimens. They prepared both 50 and 90  $\mu\text{m}$  PEO oxide-coated samples for bare and shot-peened conditions. The surface characterization of the coatings exhibits a crater/pancake surface morphology. Figure 5 represents the SEM of the plain MAO coating on the bare and shot-peened substrate. This is due to the subsequent melting+oxidation and quenching of the molten alumina from the discharge channel. Irrespective of shot-peening, the pancake diameters increased for 90  $\mu\text{m}$  coated samples. The barrier oxide coating exhibited increased impedance and polarization resistance and sub-surface compressive residual stresses.

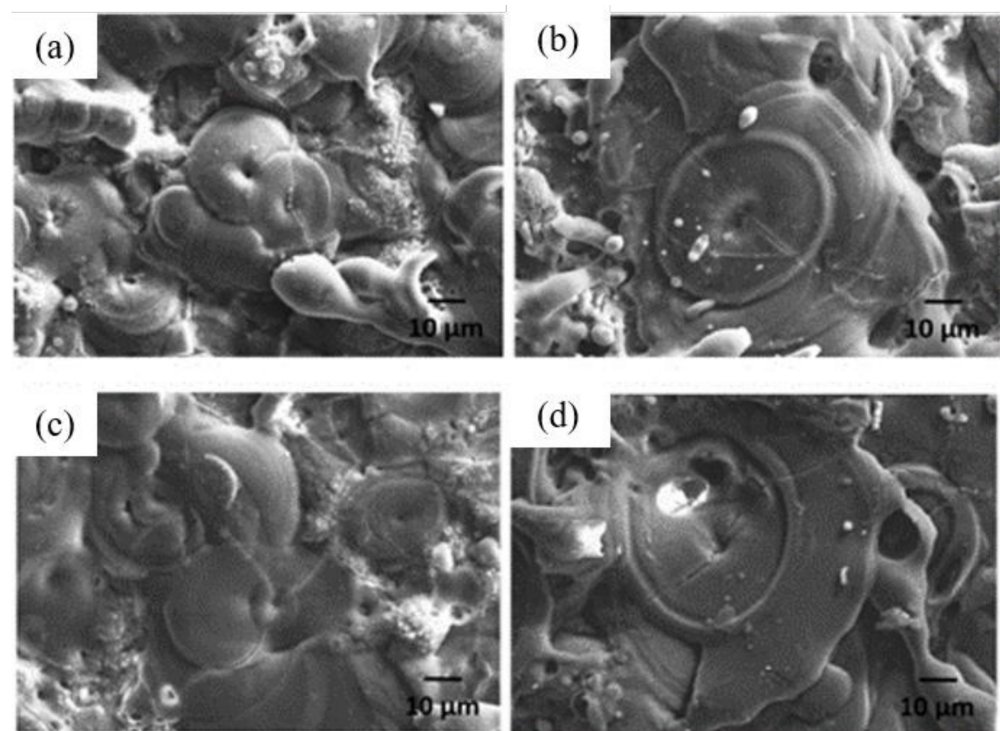


**Figure 5.** SEM micrograph of plain MAO coating of (a) 50  $\mu\text{m}$  and (b) 90  $\mu\text{m}$ ; shot peened + MAO coating of (c) 50  $\mu\text{m}$  and (d) 90  $\mu\text{m}$  coating deposited on 6061-T6. Reproduced with permission from [63]. Copyright Elsevier, 2021.

#### 4.2. PEO of 6063 Al Alloys

Sobolev et al. [42] have investigated the corrosion resistance of the PEO coatings generated on the 6063 Al alloy. They have used phosphate-based electrolytes containing glycerin. They demonstrated that the addition of glycerin to the electrolyte increases the solution's stability and helps in obtaining a uniform, dense coating and these factors enhance the corrosion resistance of the coatings. Zahng et al. [64] explored the effect of current densities during PEO of 6063 Al alloy on the microstructure and corrosion resistance of the PEO coatings.

Chen et al. [48] explored the effect of the addition of graphene particles during the PEO process. They noted that the graphene particles reduce the breakdown voltage of the oxide layer on the surface and promote coating formation. When the graphene concentration is on the lower side, it fills the pores formed on the coating surface. When the graphene concentration is higher, cracks appear on the oxide coating. The corrosion resistance of the PEO coating improved with the addition of graphene particles.

#### 4.3. PEO of 6082 Al Alloys

Malayoglu et al. [65] used PEO to create an oxide coating on the AA6082 alloy, and further, they studied their mechanical and tribological properties. The coating consisted of crystalline  $\alpha\text{-Al}_2\text{O}_3$  and  $\gamma\text{-Al}_2\text{O}_3$  phases, and after the PEO coating, the samples exhibited improved hardness and elastic modulus values. Further, PEO-coated samples also demonstrated increased adhesion strength and excellent wear resistance. Typical features of a PEO coating are presented by Shrestha et al. [66]. Though they had taken the AA6082 alloy as the substrate (Figure 6), the features remain true for the PEO coating and any 6xxx series alloy. It comprises several large pores of 5–10  $\mu\text{m}$ , microscale pores of size  $<2 \mu\text{m}$ , along with shrinkage cracks created during PEO. The coating is relatively dense (though some porosity exists), and the microstructure comprises circular fused ceramic grains formed by quenching of molten pools of oxide material.

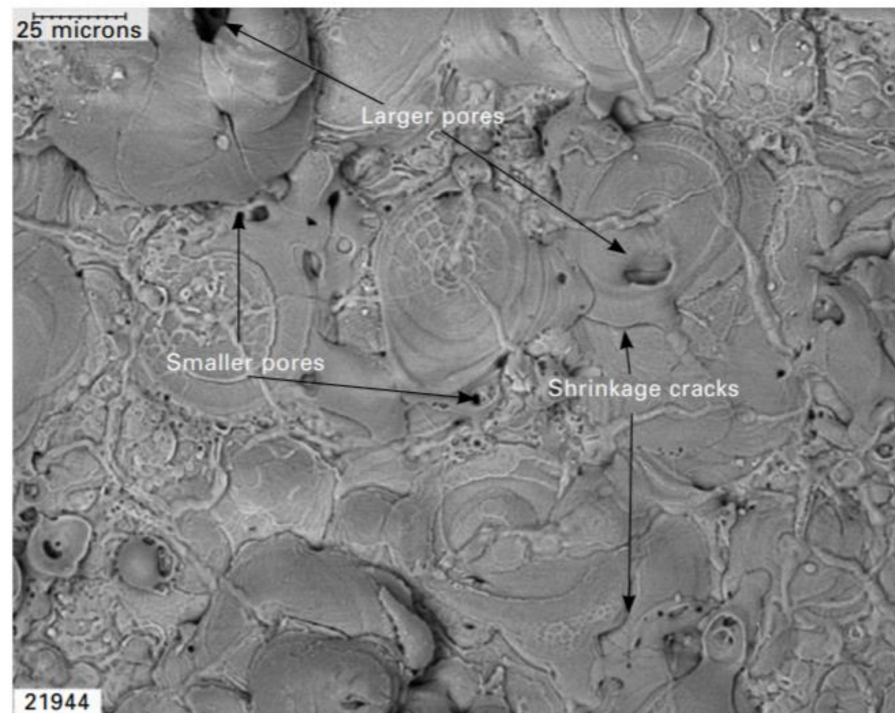


**Figure 6.** SEM micrograph of PEO surface on AA6082. Reproduced with permission from [66]. Copyright Elsevier, 2010.

Yurekturk et al. [67] explored the effect of carbon nanotubes (CNTs) on the electrolyte during PEO of the 6082 alloys. It is observed that the addition of CNTs generates an alumina coating with less porosity. CNTs also promote increased  $\alpha$ -alumina content in the oxide coating. This coating had higher hardness and wear resistance than the coating produced without CNT addition to the electrolyte. The coating is also expected to have better lubrication properties. Yan et al. [68] have explored the long-term corrosion and wear protection of 6082 Al alloy subjected to the PEO process. The electrolyte was a mixture of sodium silicate, sodium phosphate, potassium hydroxide, ammonium vanadate, and deionized water. A top layer of  $Ti_3C_2Tx$ -epoxy coating exhibited good adhesion, and it exhibited good corrosion and wear resistance.

Overall, the PEO process is a highly promising surface modification technique suitable for light metals in general and 6xxx series Al alloys in particular. With more developments, the coatings are expected to have more functional properties, and this will encourage more and more applications for 6xxx series Al alloys in days to come.

## 5. Friction Stir Processing

Friction stir processing (FSP) is a surface modification technology based on the principles of friction stir welding (FSW), which is helpful in enhancing specific properties by facilitating local microstructural change [69,70]. FSW is used to join more than one plate or sheet, whereas FSP is used to process the base material to enhance its surface properties by refining the grain structure, adding a second phase material, altering the distribution of second phase material, etc. Figure 7 demonstrates the schematics of the FSP. Here, a rotating tool with or without a pin and shoulder would be inserted into the monolithic or substrate materials. It would rotate and move with respect to the substrate, causing intense plastic deformation, material mixing, refinement, temperature rise, etc., leading to the desired surface modification. It has multiple benefits, such as solid-state microstructural evolution, fine-tuning of mechanical properties using optimized tool design and process variables, controlling the location and depth of the processed zones, the absence of deleterious gas production, and minimum materials distortion. Friction stir processing could be employed

with or without the addition of second phase particles. When a second phase material is added during FSP, the second phase may act as a reinforcement phase, pinning point, and controlling point for grain refinement, may react with the substrate to cause a new strengthening phase, etc. [71–73].

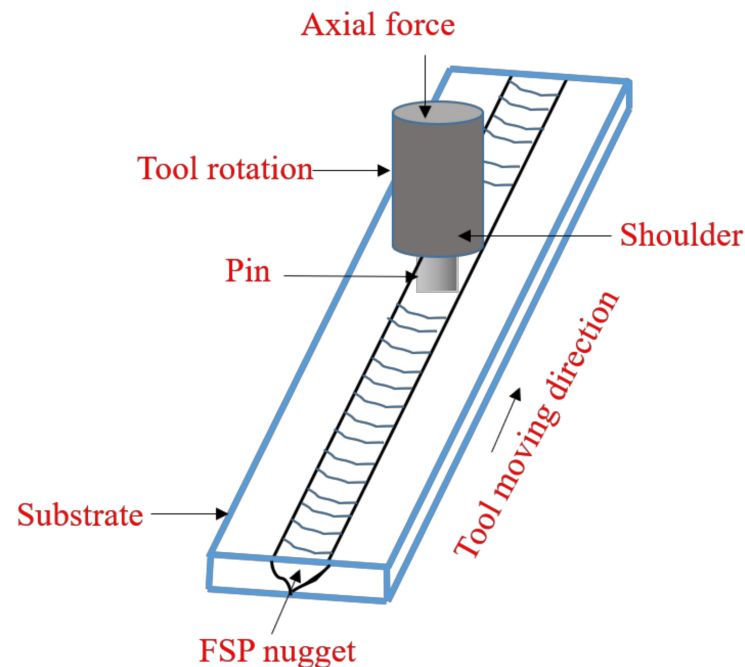


**Figure 7.** Schematic of friction stir processing.

### 5.1. FSP without Any Additions

The purpose of FSP without any addition is generally to eliminate defects, such as coarse grains, porosity, etc. Additionally, FSP improves grain refinement, ductility, and superplasticity. Singh and Kandikonda [74] reviewed important process variables affecting friction stir processing. Mehta and Badheka [75] explored the effect of FSP on the tribological properties of Al6061-T6 alloy. The focus of the investigation was the influence of the number of FSP passes and the direction of processing passes. The authors observed better wear resistance on the FSP'ed component compared to the unprocessed sample. They also reported improvement in wear resistance with the number of passes. With the reversal in the processing direction, wear resistance increases. It is attributed to the extra refinement of grains and more dispersion of the precipitates on the reversal of the FSP direction. Zhao et al. [76] explored the effect of FSP on the microstructure development and mechanical properties of the 6063 Al alloy. Figure 8 illustrates the inverse pole figure and grain boundary map of 6063 Al alloy and FSP'ed 6063 Al alloy.

They noted that an increase in the tool rotation speed increases grain refinement in the stir zone. Multi-pass stirring produces more refined grains than single-pass stirring on the same line. The mechanical properties were weaker at a lower rotation speed, but mechanical properties exceeded that of the base material at a higher speed.

Patel et al. [77] reviewed FSP as a means to achieve superplasticity behavior in Al alloys. Zarghani et al. [78] investigated the effectiveness of friction stir processing for enhancing metal properties of the 6082-T4 alloy. They noted that the intense plastic deformation occurring during FSP causes dynamic recrystallization, producing an ultrafine grain structure. Additionally, the hardness of the alloy increased with a decrease in the tool rotation speed. Kumar [79] explored the effect of superimposition of ultrasonic vibrations and the FSP on 6063 alloys. The rotational speed and processing speeds were varied. It was observed that ultrasonic vibrations help to generate heat in the stirred zone and encourage material flow. It reduces the quantum of axial force and transverse force required for effec-

tive processing. Senthilkumar et al. [80] explored the effect of the multiple passes on the microstructural modification in AA6082 alloy. They explored the effect of various process parameters, such as rotational tool speed, number of passes, etc., on the microstructural and mechanical changes. Heat generation in the stirred zone was monitored using an infrared (IR) camera. They noted considerable improvement in the tensile and impact strength, whereas the improvement in the hardness was marginal.

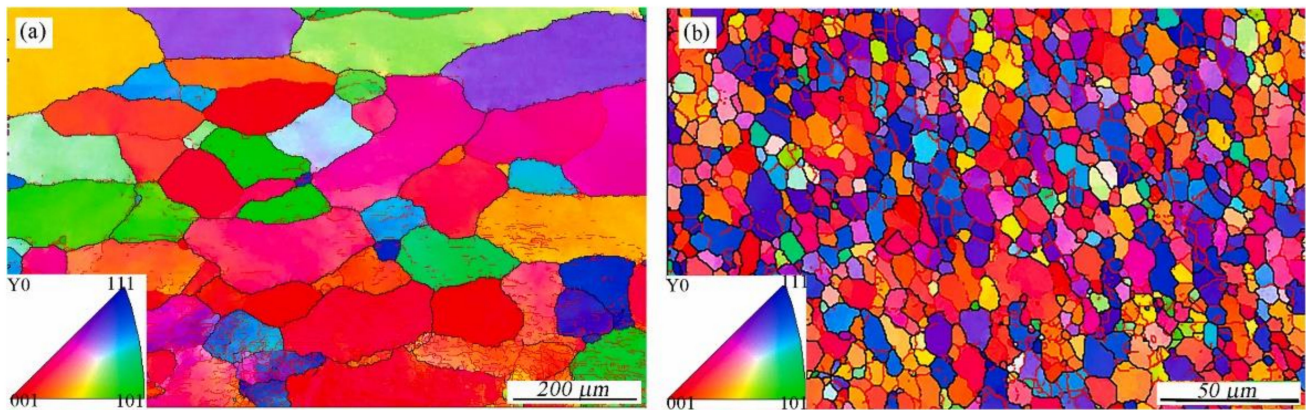


**Figure 8.** Grain boundary identification using electron backscattered diffraction in (a) the base metal AA 6063 and (b) the FSP'ed region. Reproduced with permission from [76]. Copyright Elsevier, 2019.

Fadhilah and Asi [81] explored the effect of FSP on the microstructure, aging kinetics, and microhardness behavior of the AA6082 alloy. They noted that the stirred zone undergoes dynamic recrystallization, leading to refined grains. When subjected to aging, the same region became still finer due to recovery and recrystallization. In addition, there was a texture change due to recrystallization. Sarvaiya and Singh [82] subjected rolled plates of AA6082-T6 alloy to FSP. They explored the effect of rotational tool speed, processing speed, and tilt angle on surface defects, surface appearance, heat generation, and flash formation. The study concludes that the possibility of excess heat and insufficient heat formation limits the range of processing parameters. When processing parameters go out of these bounds, the process can create a defective material.

### 5.2. FSP with the Addition of Surface Alloying Elements

In this methodology, during friction stir processing, an element or an alloy that tends to dissolve in the substrate will be added, either by making a groove or by drilling holes in the substrate or by applying in the form of deposition on the surface. Though this type of alloying is explored considerably for Al alloys belonging to the 2xxx, 5xxx, and 7xxx series, it is relatively less explored in the case of 6xxx series alloys. Mane and Hosamani [83] used copper as an additive during the FSP of AA6061 alloy. Before FSP, the copper powder was thermally sprayed on the grooves made on Al6061 alloy. Defect-free stirred zone was observed during FSP when the traveling speed was low. The stirred zone was exhibiting grain refinement. The stirred zone was exhibiting accelerated aging kinetics to precipitate  $\text{Al}_2\text{Cu}$ . The stirred zone exhibited increased hardness and was attributed to the precipitation of Al-Cu phases. Balakrishnan et al. [84] used FSP to alter the structure at the surface of the cast Al 6061+ $\text{Al}_3\text{Fe}$  composite. They observed that defects such as coarse grains, pores, segregation of sharp particles, etc., could be eliminated using FSP. As-cast microstructures of AA6061 +  $\text{Al}_3\text{Fe}$  composites containing different fractions of  $\text{Al}_3\text{Fe}$  are presented in Figure 9.

Microstructural changes in the same composite after friction stir processing can be easily visualized using micrographs presented in Figure 10. The microstructural changes due to FSP improve mechanical properties, such as strength and ductility.

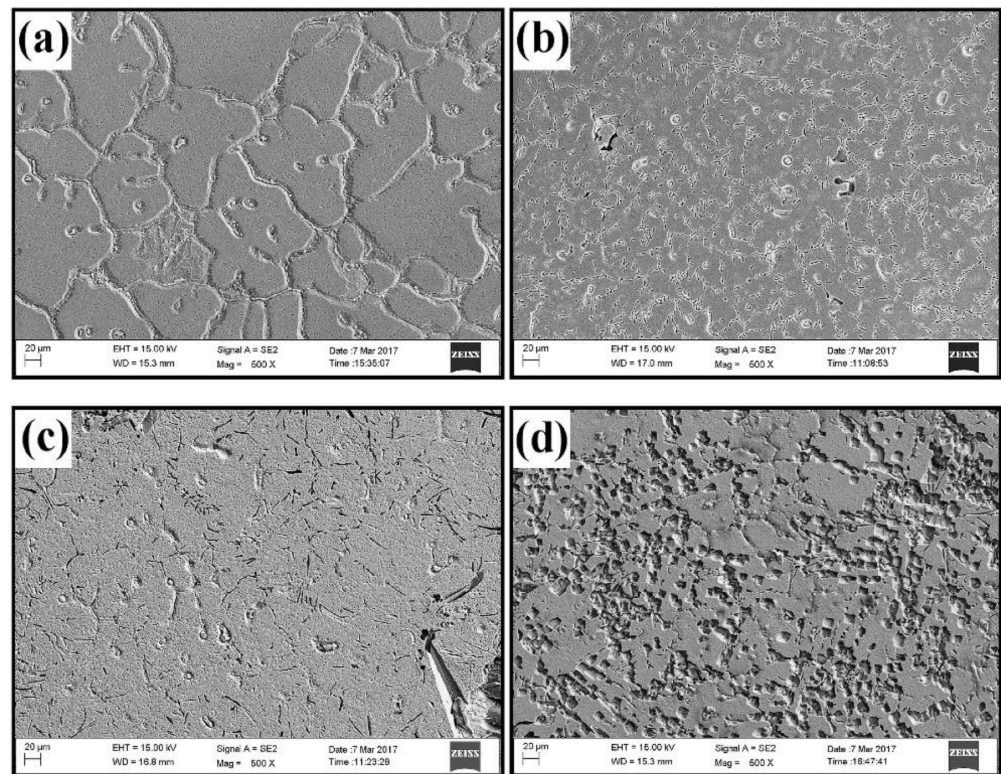


**Figure 9.** Micrographs of cast AA6061/Al<sub>3</sub>Fe composites containing different amounts of Al<sub>3</sub>Fe: (a) 0 (b) 5, (c) 10, and (d) 15 vol. % of Al<sub>3</sub>Fe. Reproduced with permission from [84]. Copyright Elsevier, 2019.

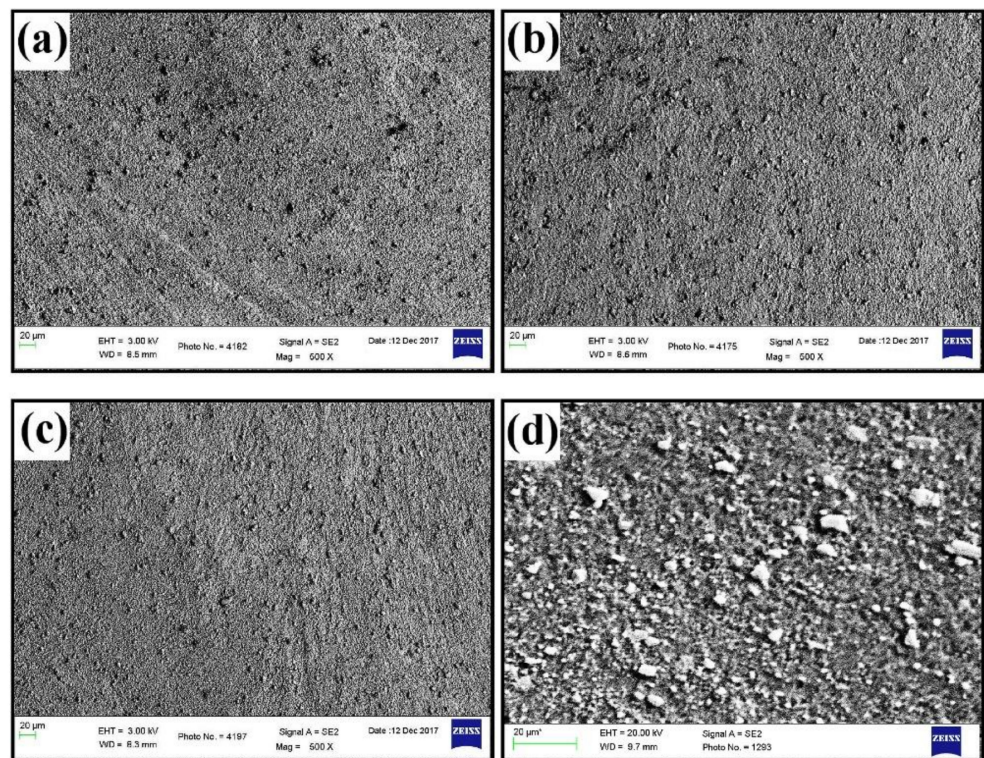


**Figure 10.** Micrographs of friction stir processed AA6061+Al<sub>3</sub>Fe composites: (a) 0, (b) 5, (c) 10, and (d) 15 vol. % of Al<sub>3</sub>Fe reinforcements. Reproduced with permission from [84]. Copyright Elsevier, 2019.

### 5.3. FSP with the Addition of Hard Reinforcement Phases

Generally, composites exhibit high strength, high modulus, improved fatigue behavior, creep and wear resistance, and a prospective structural material. However, these composites exhibit low ductility and toughness, reducing their prospect of applications. In applications such as wear and fatigue, where surface properties are essential, an appropriate alternative would be to convert the material at the surface as a composite by adding the reinforcement particles [71–85]. Figure 11 presents a micrograph of the commercial Al alloy with the surface-modified SiC-reinforced composite, using the FSP process. Various types of hard reinforcement phases are being explored in this domain. Some of them are  $\text{Al}_2\text{O}_3$ , SiC,  $\text{B}_4\text{C}$ , graphite,  $\text{TiB}_2$ , etc. These particles could be microscale or nanoscale in size. In addition to composite fabrication, FSP is also being used to develop functionally graded materials on the surface of metallic substrates.

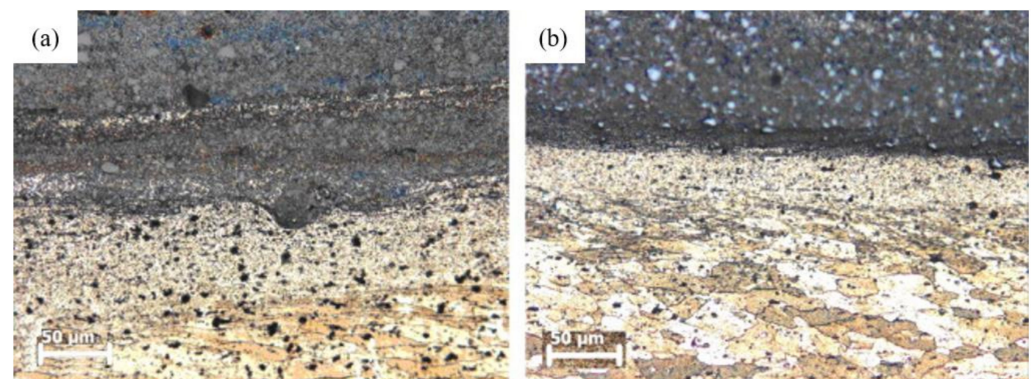


**Figure 11.** Successful composite formation at the surface, using FSP at two different travel speeds. Base material here is commercial Al: (a) lower speed; (b) higher speed. Reproduced with permission from [71]. Copyright Elsevier, 2011.

Functionally graded materials are materials with specific functional characteristics, which are obtained due to changes in reinforcement volume, orientation, density, materials shape, etc. These variations bring specific functional characteristics to the substrate surface [72]. Various researchers explored and reviewed the possibility of adding reinforcement particles to the surface of 6xxx series alloys using friction stir processing. It also covers the improvisation of mechanical and surface properties.

Many researchers have explored the effects of the addition of SiC of various size scales during friction stir processing. Choi et al. [86] explored the effect of the addition of SiC particles during the FSP of AA6061-T4 alloy. They observed grain refinement due to the presence of SiC during stirring. A combination of grain refinement and SiC particles increased the hardness of the stirred zone. Eftekharinia et al. [87] processed Al6061 reinforced with SiC particles of 40  $\mu\text{m}$  size using FSP and obtained a surface composite. They explored the effect of pin geometry and the number of passes on microstructure, wear rate, and microhardness variation. They noted that with the increase in the number of passes, the distribution of particles became more uniform, and grain size was reduced. Additionally, pin geometry and the number of passes played an essential role in grain refinement and distribution of the particles. The pins with square and cylindrical profiles exhibited minimum wear damage during FSP.

Researchers have investigated the effect of the addition of nanoscaled SiC particles to 6xxx series Al alloys during FSP. Salehi et al. [88] produced AA6061-SiC nanocomposites using FSP. They explored the effect of process variables, such as rotational speed, traverse speed, pin profile, and tool penetration depth, on the ultimate tensile strength. Using the design of the experiment method, they identified tool rotational speed as the parameter of maximum influence. Mehdi and Mishra [89] fabricated AA6082 matrix + SiC nanoparticles reinforced composites. They considered a fixed tool rotation speed, feed rate, and tilt angle. The number of FSP passes was the variable. Fragmentation of particles and uniform

distribution of SiC particles was observed after the 5th pass. The UTS of the composite increased progressively with the number of passes, and it is attributed to grain refinement, fragmentation of SiC particles, and their improved dispersion. Salehi et al. [90] prepared a graded Al-SiC composite by using SiC powders of 50 nm size using multistep friction stir processing. The matrix material was 6061 alloy. The grading was with respect to the percentage of SiC nanoparticles, and its range was 0 to 18 wt.%. The maximum hardness achieved was five times that of the base material. Furthermore, they could correlate the hardness values to the inverse of particle spacing.

Similarly, researchers have investigated the effect of the addition of micrometer and nanometer-sized SiO<sub>2</sub> particles during FSP. Zuhailawati et al. [91] have used amorphous silica obtained from rice husk ash to reinforce 6061 Al alloy. They noted that the presence of silica restricts grain growth in the Al matrix. The hardness of the alloy was sensitive to heat generated during FSP. Mazaheri et al. [92] explored the effect of multiple passes during FSP and nanoparticles of SiO<sub>2</sub> on Al6061-based nanocomposite formation. Properties such as microhardness, wear resistance, and corrosion resistance was investigated. They noted that the higher the number of passes, the distribution of nanoparticles would be better, and it results in an improvement in wear resistance. They also observed that the application of FSP led to coarsening of Mg<sub>2</sub>Si and, in turn, reducing strength and corrosion resistance.

A couple of research investigations focus on using Al<sub>2</sub>O<sub>3</sub> as the reinforcement during FSP. Devaraju et al. [93] explored the effect of reinforcement particles (SiC and Al<sub>2</sub>O<sub>3</sub>, separately) and rotational speed on making 6061-based surface composites. They used reinforcement particles of 5 µm size and found uniformly distributed particles. In addition to the reinforcement, they made square grooves of 3 mm width and 3 mm depth. The composite had improved hardness and wear resistance. Qu et al. [94] prepared Al 6061-T651 alloy-based composite using sub-micrometer-sized Al<sub>2</sub>O<sub>3</sub> and SiC particles (separately) up to 3 mm thick. They added the Al<sub>2</sub>O<sub>3</sub> reinforcement phase up to 20–30 by vol.%. The composite improved friction and wear resistance by 40 and 90% compared to bare Al 6061 alloys. Wear resistance was further increased by additional heat treatment. Naresh et al. [95] added nano-alumina particles (40–50 nm) as reinforcement during the FSP of Al 6061 alloy. They reported a significant improvement in microhardness. Guo et al. [96] fabricated AA6061-based nanosized Al<sub>2</sub>O<sub>3</sub>-reinforced nanocomposites using FSP. They used 2 mm deep and 1 mm diameter holes for adding nanopowders. Volume fractions of powders were approximately 14%. They noted that the added particles act as pinning sites and help in controlling the composite's grain size. As a result, the composite significantly increased microhardness and tensile strength.

Other than SiC, SiO<sub>2</sub>, and Al<sub>2</sub>O<sub>3</sub>, other hard oxides are also explored as a reinforcement phase for modifying the 6xxx series Al alloys. Kheirkhah et al. [97] prepared a boron nitride (BN)-reinforced Al6061-T6 surface composite by FSP. By employing four passes, they could achieve a uniform dispersion of BN particles. Due to the combined effect of the pinning effect from the hard BN particles and reduced grain size, the microhardness increased drastically in the FSP zone. Additionally, increasing the number of FSP passes increased the mechanical properties. Corrosion measurements also indicated the improvement with FSP and the addition of BN particles. Patel et al. [98] modified the surface of the Al alloy 6063 using fine ZrO<sub>2</sub> powder and friction stir processing. ZrO<sub>2</sub> powder was spread finely due to FSP. Both microhardness and tensile strengths of the FSP zone progressively improved with the increased number of FSP passes.

Another important aspect of the fabrication of a composite using FSP is the way in which the reinforcement phase is handled during the process. Rathee et al. [99] compared the strengths of various particle addition methods during FSP to fabricate a surface composite, and they observed that the use of grooves to deposit reinforcements exhibits homogenous surface composite.

Another notable direction of research activity is using multiple reinforcement phases to make a hybrid composite with 6xxx series alloy as the matrix material. Palanivel et al. [100] successfully fabricated AA6082-based hybrid nanocomposites with TiB<sub>2</sub> and BN particles,

which is shown in Figure 12. The performance of the hybrid nanocomposite was compared with AA6082, AA6082 + BN, and AA6082 + TiB<sub>2</sub>. It was noted that under optimum conditions, the reinforcement particles were homogeneously dispersed within the stir zone. The interface between the particles and the matrix was excellent, and there was extensive grain refinement in the matrix. The addition of BN nanoparticles enhanced the wear resistance of the 6082-TiB<sub>2</sub> composite. They also reduced the wear of the counter material.

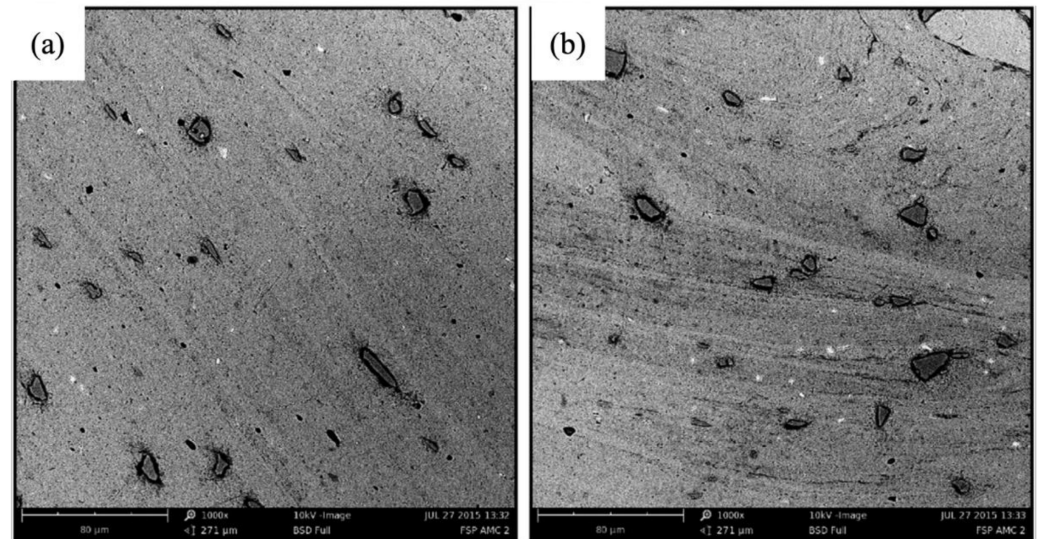


**Figure 12.** Micrographs of AA6082-based hybrid composites (a) and (b) at two different locations showing coarse particles: TiB<sub>2</sub> and fine particles: BN Reproduced with permission from [100]. Copyright Elsevier, 2016.

Barenji et al. [101] fabricated AA6061-based hybrid composites using Al<sub>2</sub>O<sub>3</sub> and TiB<sub>2</sub> powders through FSP. The effect of several passes on the microstructure, wear and hardness was explored. They noted that an increase in the number of passes improved the dispersion of the particles, which, in turn, improved the hardness and wear resistance. Anvari et al. [102] prepared Al–Cr–O hybrid nanocomposite on the surface of the Al6061 by FSP. They noted that the nanocomposite has higher wear resistance compared to plain 6061-T6 alloy. Anandhakumar et al. [103] fabricated Al 6061 alloy-based hybrid surface composites using Al oxide, BC, BN, and graphite on an equal volume basis. They could achieve uniform dispersion of reinforcement particles and good bonding between the matrix and the reinforcement particles. They summarized that BC and Al oxide addition improves mechanical properties compared to other reinforcement particles. Dinesh et al. [104] prepared an Al 6063-based hybrid composite consisting of B<sub>4</sub>C and SiO<sub>2</sub> with different weight fractions. The friction tool was a non-consumable tool made using HSS. The results indicated a uniform distribution of particles and refinement in grain size.

## 6. Friction Surfacing

Friction surfacing is a solid-state deposition method that can coat similar and dissimilar materials. It allows the deposition of coatings materials in a layered, non-fusion manner. In this method, the material to be deposited is used as a consumable tool and pressed against the substrate surface with a normal force. Simultaneously, it is rotated on the substrate surface resulting in frictional heating at the interface. The rise in pressure and the temperature at the interface facilitate the formation of a viscoelastic zone, and bonding develops between the substrate and the deposit [105,106]. The schematic of the friction surfacing is represented in Figure 13.

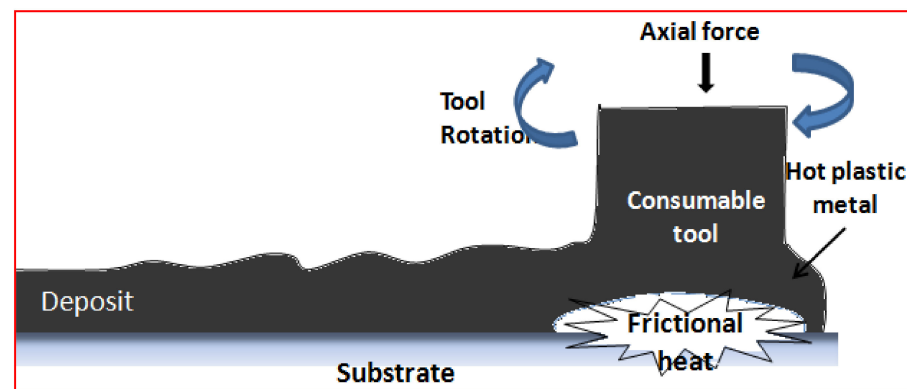


**Figure 13.** Schematic presentation of friction surfacing process. Reproduced with permission from [106]. Copyright Elsevier, 2014.

Friction surfacing is a coating technology for materials carried out under solid-state. Due to this, it imparts reduction in heat input compared to fusion-based processes, and hence heat-affected zone (HAZ) is small, and distortion of the parts is minimum [107,108]. It is reported that the deposition efficiency is a function of energy input for a fixed volume and affects the deposited material. The deposition geometry is also reported as a function of the process parameters and temperature evolution during friction surfacing [109,110]. From the direction of friction surfacing, 6xxx series alloys as the tool material are more explored than 6xxx series alloys as the substrate material [109–113]. In this review, the use of the 6xxx series as the substrate material is considered. Yuvaraj [114] explored the effect of adding  $ZrO_2$  during friction surfacing to make a surface composite on the surface of 6082 Al alloy. They noted improved hardness and tribological properties after making the surface a composite.

## 7. Laser Cladding

Laser-based surface modification techniques are widely applied in diverse fields of applications to enhance the surface integrity and surface mechanical properties of metals and alloys. This includes laser shock peening [115], laser cladding [116], laser remelting [117], and laser surface alloying [5]. Among these techniques, laser cladding is a superior surface strengthening and repair technique introduced in the early 1980s. The coating can be made in a single stage or double stage process. In a single-stage process, the coating material in a powder form is preplaced in the substrate material or injected either in coaxial/off-axis mode or fed as a wire into the molten melt pool created on the substrate surface [8,118–120]. In a two-stage laser cladding, a slurry deposited on the substrate material is melted with the help of a laser beam. Figure 14 demonstrates the schematic diagram of the coaxial laser cladding system. In laser cladding, a high-power density laser beam scans over the surface of the substrate material to form a molten melt pool when the powder is injected onto the substrate through the nozzle with the help of carrier gas. The laser and powder interaction causes the powder to enter a melt pool, forming a cladding layer. Due to laser irradiance, there will be a sharp temperature gradient in the clad layer, interface, and surface of the substrate material, promoting grain refinement. In this process, a shielding gas is employed to prevent oxidation in the melt pool. Each of these processes has its advantages as well as disadvantages. Laser cladding using powder injection is the widely adopted technique among the mentioned process [121]. Laser cladding leads to the formation of a uniform coating on the substrate material with no signs of crack, and they offer enhanced mechanical properties [122]. Laser cladding has added advantages of high energy density, enhanced metallurgical bonding with the substrate, uniform coating thickness, high compactness, and high performance in comparison with physical vapor deposition (PVD) and chemical vapor deposition (CVD) techniques [123,124].

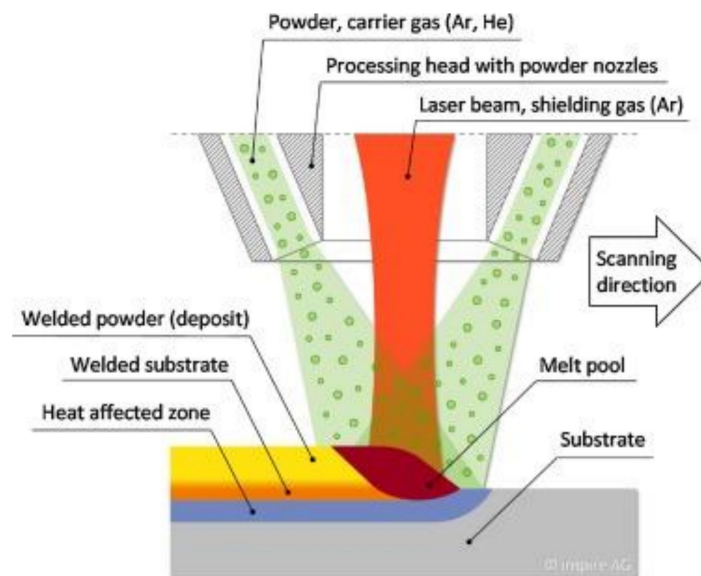


**Figure 14.** Schematic showing coaxial laser cladding system. Reproduced with permission from [120]. Copyright Elsevier, 2018.

Grohl et al. [8] performed laser cladding through the off-axis powder injection of Al alloy 6061 powder on a 6061–T6511 substrate material using a 4 kW high power diode laser. The authors used different power, scan speed, and feed rate in this experiment and performed several experiments to optimize the parameters. The authors summarized that power of 3625 W, feed of 0.18 g/s, and a scan speed of 2.5 mm/s can provide the highest clad and maximum hardness in the heat-affected region (HAZ). The authors reported fine and large precipitates in the cladding, which accounts for the maximum hardness in the HAZ. The nickel-based cladding was widely used for surface strengthening because of the wear-resistance and high-temperature properties. Wang et al. [125] laser clad Ni60 layers with three different rare earth oxides, such as  $\text{CeO}_2$ ,  $\text{Y}_2\text{O}_3$ , and  $\text{La}_2\text{O}_3$ , with a varying weight percent on Al 6063 alloys. The authors observed that Ni60 cladding layers that do not contain rare earth oxides showed many pinholes and furrow gullies in the direction of cladding, and these are detrimental. This is attributed to the poor mobility of the molten pool and the entrapment of gases in the molten pool. However, the addition of rare earth oxides showed a remarkable reduction in surface pores and enhancement in surface roughness. The surface density of the cladding layer with rare earth oxides was high. This is due to the presence of rare earth oxides that enhanced the convection in the molten melt pool, promoting the uniform distribution of cladding elements and, subsequently, easy removal of trapped gases from the molten pool. The addition of rare earth improved surface hardness and refined microstructure of Ni60 layers compared to Ni60 layers without rare earth on the substrate. Wang et al. [126] studied the influence of rare earth on tribological properties of the nickel-based claddings on Al 6063 alloys and compared it with nickel-based cladding without rare earth. The authors divulged that the wear volume loss of nickel-based claddings containing rare earth elements was  $0.0974 \text{ mm}^3$ , while the cladding layers added with  $\text{La}_2\text{O}_3$ ,  $\text{Y}_2\text{O}_3$  and  $\text{CeO}_2$  are  $0.0018$ ,  $0.0159$  and  $0.0031 \text{ mm}^3$ , which is one magnitude less than the nickel-based cladding without rare earth. The wear depth and wear resistance were superior for nickel-based claddings containing rare earth elements. The improvement in wear resistance can be correlated with hardness as per Archard's equation [127]. This equation demonstrates that the wear volume is inversely related to the hardness.

$$Q = K \frac{Wx}{H} \quad (1)$$

where  $Q$  is the wear volume,  $K$  is the wear coefficient,  $W$  is the normal load,  $x$  is the sliding distance, and  $H$  is hardness. The authors reported a 75% improvement in hardness when rare-earth were incorporated in the nickel-based cladding. The coefficient of friction (COF) was similar for both the claddings initially, and COF increased for cladding that does not contain rare earth. The authors reported the lowest COF for the cladding that has rare earth. This is because of the compact dendritic microstructure with refined grains and the absence of pores in the clad. Among the various rare earth oxides in the nickel cladding, the cladding that contains 5 wt.%  $\text{CeO}_2$  showed the lowest COF. Figure 15 demonstrates the CoF of nickel cladding that has rare earth and without rare earth.

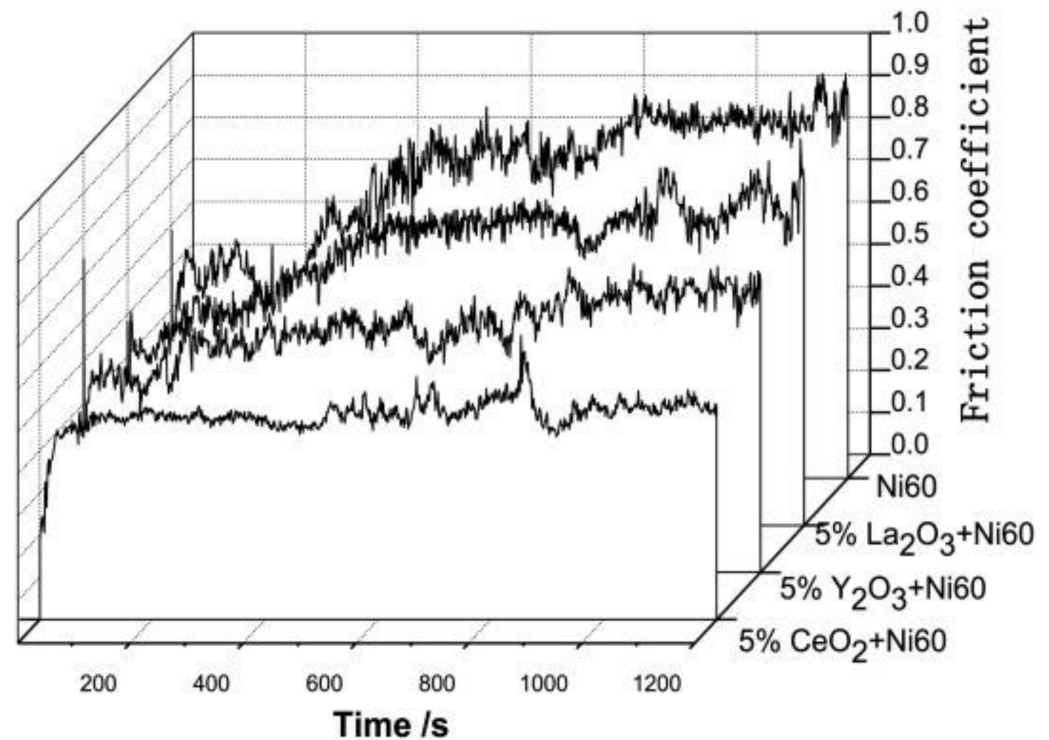


**Figure 15.** COF of the nickel cladding layers containing rare earth and without rare earth. Reproduced with permission from [126]. Copyright Elsevier, 2017.

The figure shows that the presence of rare earth in the laser cladding reduced the COF and improved the wear resistance. Thus, laser cladding can significantly enhance the surface mechanical properties of the substrate materials.

Overall, laser cladding is a vital surface modification technique for Al alloys that can enhance surface mechanical properties and integrity, ultimately improving components' performance in extreme conditions.

## 8. Conclusions

This review article elucidated a comprehensive discussion on various surface modification techniques for 6xxx series Al alloys. Surface modification techniques can enhance the surface mechanical properties and surface integrity of the component. Various surface modification methods such as anodizing, plasma electrolytic oxidation, friction stir processing, friction surfacing, and laser cladding were considered in this review. This process can effectively improve the surface mechanical properties of Al alloys used in the medical, aerospace, automotive, oil, and gas industries. This study also incorporated current state-of-the-art of these surface modification techniques on the most widely used 6xxx series Al alloys. The mechanism and most influential process parameters pertaining to these processes were explained for predominantly used 6xxx series Al alloys. The effect of these processes on mechanical properties and microstructural features was summarized.

This review article can offer better insights when choosing the surface modification for 6xxx series Al alloys for diverse applications.

**Author Contributions:** Conceptualization, K.U.B.; methodology, K.U.B.; writing—original draft preparation, K.U.B., D.B.P., S.B.K., M.J. and P.L.M.; writing—review and editing, K.U.B., D.B.P., S.B.K., M.J. and P.L.M.; supervision, K.U.B. and P.L.M. All authors have read and agreed to the published version of the manuscript.

**Funding:** This research received no external funding.

**Institutional Review Board Statement:** Not applicable.

**Informed Consent Statement:** Not applicable.

**Data Availability Statement:** Data sharing is not applicable to this article.

**Acknowledgments:** The authors acknowledge the Metallurgical and Materials Engineering, National Institute of Technology, Karnataka and Department of Mechanical Engineering, University of Nevada, Reno, for providing all research facilities.

**Conflicts of Interest:** The authors declare no conflict of interest. The funders had no role in the design of the study; in the collection, analyses, or interpretation of data; in the writing of the manuscript; or in the decision to publish the results.

### Abbreviations

AC	Alternating Current
BC	Boron Carbide
BN	Boron Nitride
CNT	Carbon nanotube
DC	Direct Current
FSP	Friction Stir Processing
FSW	Friction Stir Welding
SEM	Scanning Electron Microscopy
PEO	Plasma Electrolytic Oxidation
UTS	Ultimate Tensile Strength
YS	Yield Strength

### References

1. Riquelme, A.; Rodrigo, P.; Escalera-Rodríguez, M.D.; Rams, J. Corrosion Resistance of Al/SiC Laser Cladding Coatings on AA6082. *Coatings* **2020**, *10*, 673. [[CrossRef](#)]
2. Bodunrin, M.O.; Alaneme, K.K.; Chown, L.H. Aluminium Matrix Hybrid Composites: A Review of Reinforcement Philosophies; Mechanical, Corrosion and Tribological Characteristics. *J. Mater. Res. Technol.* **2015**, *4*, 434–445. [[CrossRef](#)]
3. Liu, H.; Zhao, G.; Liu, C.; Zuo, L. Effects of Different Tempers on Precipitation Hardening of 6000 Series Aluminium Alloys. *Trans. Nonferrous Met. Soc. China* **2007**, *17*, 122–127. [[CrossRef](#)]
4. Tisza, M.; Lukács, Z. High Strength Aluminum Alloys in Car Manufacturing. *IOP Conf. Ser. Mater. Sci. Eng.* **2018**, *418*, 012033. [[CrossRef](#)]
5. Chi, Y.; Gu, G.; Yu, H.; Chen, C. Laser Surface Alloying on Aluminum and Its Alloys: A Review. *Opt. Lasers Eng.* **2018**, *100*, 23–37. [[CrossRef](#)]
6. Dzhurinskiy, D.V.; Dautov, S.S.; Shornikov, P.G.; Akhatov, I.S. Surface Modification of Aluminum 6061-O Alloy by Plasma Electrolytic Oxidation to Improve Corrosion Resistance Properties. *Coatings* **2021**, *11*, 4. [[CrossRef](#)]
7. Rahman, M.; Ariffin, A.; Jamaludin, B.N.J.B.N.; Haron, C. Fatigue behaviour of 6000 series aluminium alloys on cylinder block of a free piston linear engine using total life approach. *J. Mek.* **2006**, *21*, 1–15.
8. Grohol, C.M.; Shin, Y.C.; Frank, A. Laser Cladding of Aluminum Alloy 6061 via Off-Axis Powder Injection. *Surf. Coat. Technol.* **2021**, *415*, 127099. [[CrossRef](#)]
9. Sweet, G.A.; Brochu, M.; Hexemer, R.L.; Donaldson, I.W.; Bishop, D.P. Consolidation of Aluminum-Based Metal Matrix Composites via Spark Plasma Sintering. *Mater. Sci. Eng. A* **2015**, *648*, 123–133. [[CrossRef](#)]
10. Kushwaha, A.K.; John, M.; Misra, M.; Menezes, P.L. Nanocrystalline Materials: Synthesis, Characterization, Properties, and Applications. *Crystals* **2021**, *11*, 1317. [[CrossRef](#)]
11. John, M.; Ralls, A.M.; Dooley, S.C.; Thazhathidathil, A.K.V.; Perka, A.K.; Kuruveri, U.B.; Menezes, P.L. Ultrasonic Surface Rolling Process: Properties, Characterization, and Applications. *Appl. Sci.* **2021**, *11*, 10986. [[CrossRef](#)]

12. Miller, W.S.; Zhuang, L.; Bottema, J.; Wittebrood, A.J.; De Smet, P.; Haszler, A.; Vieregge, A. Recent Development in Aluminium Alloys for the Automotive Industry. *Mater. Sci. Eng. A* **2000**, *280*, 37–49. [[CrossRef](#)]
13. Kaufman, J.G. *Introduction to Aluminum Alloys and Tempers*; ASM International: Russell Township, OH, USA, 2000; ISBN 978-0-87170-689-8.
14. Miao, W.F.; Laughlin, D.E. Precipitation Hardening in Aluminum Alloy 6022. *Scr. Mater.* **1999**, *40*, 873–878. [[CrossRef](#)]
15. Lang, P.; Povoden-Karadeniz, E.; Falahati, A.; Kozeschnik, E. Simulation of the Effect of Composition on the precipitation in 6xxx Al Alloys during Continuous-Heating DSC. *J. Alloys Compd.* **2014**, *612*, 443–449. [[CrossRef](#)]
16. Summers, P.T.; Chen, Y.; Rippe, C.M.; Allen, B.; Mouritz, A.P.; Case, S.W.; Lattimer, B.Y. Overview of Aluminum Alloy Mechanical Properties during and after Fires. *Fire Sci. Rev.* **2015**, *4*, 3. [[CrossRef](#)]
17. Ilangovan, M.; Boopathy, S.R.; Balasubramanian, V. Microstructure and Tensile Properties of Friction Stir Welded Dissimilar AA6061–AA5086 Aluminium Alloy Joints. *Trans. Nonferrous Met. Soc. China* **2015**, *25*, 1080–1090. [[CrossRef](#)]
18. Vahdani, M.; Mirnia, M.J.; Bakhshi-Jooybari, M.; Gorji, H. Electric Hot Incremental Sheet Forming of Ti-6Al-4V Titanium, AA6061 Aluminum, and DC01 Steel Sheets. *Int. J. Adv. Manuf. Technol.* **2019**, *103*, 1199–1209. [[CrossRef](#)]
19. ASM Handbook Committee. *Properties and Selection: Nonferrous Alloys and Special-Purpose Materials*; ASM International: Russell Township, OH, USA, 1990.
20. ASM International. *Properties and Selection of Aluminum Alloys*; ASM International: Russell Township, OH, USA, 2019. [[CrossRef](#)]
21. Andreatta, F.; Terry, H.; de Wit, J.H.W. Corrosion Behaviour of Different Tempers of AA7075 Aluminium Alloy. *Electrochim. Acta* **2004**, *49*, 2851–2862. [[CrossRef](#)]
22. Buchheit, R.G.; Montes, L.P.; Martinez, M.A.; Michael, J.; Hlava, P.F. The Electrochemical Characteristics of Bulk-Synthesized Al<sub>2</sub>CuMg. *J. Electrochem. Soc.* **1999**, *146*, 4424–4428. [[CrossRef](#)]
23. Dzhurinskiy, D.; Maeva, E.; Leshchinsky, E.; Maev, R.G. Corrosion Protection of Light Alloys Using Low Pressure Cold Spray. *J. Therm. Spray Technol.* **2012**, *21*, 304–313. [[CrossRef](#)]
24. Cerchier, P.; Pezzato, L.; Gennari, C.; Moschin, E.; Moro, I.; Dabalà, M. PEO Coating Containing Copper: A Promising Anticorrosive and Antifouling Coating for Seawater Application of AA 7075. *Surf. Coat. Technol.* **2020**, *393*, 125774. [[CrossRef](#)]
25. Zhang, P.; Nie, X.; Han, L.; Hu, H. Wear Protection of Al<sub>3</sub>Si/SiO<sub>2</sub> Metal Matrix Composites by Plasma Electrolytic Oxidation (PEO) Process. *SAE Int. J. Mater. Manuf.* **2010**, *3*, 55–62. [[CrossRef](#)]
26. Sikdar, S.; Menezes, P.V.; Maccione, R.; Jacob, T.; Menezes, P.L. Plasma Electrolytic Oxidation (PEO) Process—Processing, Properties, and Applications. *Nanomaterials* **2021**, *11*, 1375. [[CrossRef](#)] [[PubMed](#)]
27. Rotshtein, V.P.; Shulov, V.A. Surface Modification and Alloying of Aluminum and Titanium Alloys with Low-Energy, High-Current Electron Beams. *J. Met.* **2011**, *2011*, 673685. [[CrossRef](#)]
28. Lorenzo-Martin, M.C.; Ajayi, O.O. Surface Layer Modification of 6061 Al Alloy by Friction Stir Processing and Second Phase Hard Particles for Improved Friction and Wear Performance. *J. Tribol.* **2014**, *136*, 044501. [[CrossRef](#)]
29. Polat, B.D.; Bilici, B.; Afşin, P.; Akyil, C.; Keles, O. A study of taguchi method to optimize 6XXX series aluminium anodic oxide film's hardness and investigation of corrosion behaviors of oxide films. In Proceedings of the 145th Annual Meeting & Exhibition TMS 2016, Nashville, TN, USA, 14–18 February 2016; Springer: Cham, Switzerland, 2016; pp. 401–408.
30. Avelar-Batista Wilson, J.C.; Grabowski, A.; Kustosik, K.; Wilson, A.D. Tartaric Acid Cross-Contamination in Post-Cascade Rinses after Sulphuric Acid Anodising (SAA): Effect on Adhesive Bond Strength of AA6060-T6 Alloy. *Int. J. Adhes. Adhes.* **2018**, *81*, 30–35. [[CrossRef](#)]
31. Knudsen, O.Ø.; Tanem, B.S.; Bjørgum, A.; Mårdalen, J.; Hallenstvet, M. Anodising as Pre-Treatment before Organic Coating of Extruded and Cast Aluminium Alloys. *Corros. Sci.* **2004**, *46*, 2081–2095. [[CrossRef](#)]
32. Tabrizian, N.; Hansen, H.N.; Hansen, P.E.; Ambat, R.; Møller, P. Influence of Annealing and Deformation on Optical Properties of Ultra Precision Diamond Turned and Anodized 6060 Aluminium Alloy. *Surf. Coat. Technol.* **2010**, *204*, 2632–2638. [[CrossRef](#)]
33. Short, E.P.; Bryant, A.J. A Review of Some Defects Appearing on Anodized Aluminium. *Trans. IMF* **1975**, *53*, 169–177. [[CrossRef](#)]
34. Ma, Y.; Zhou, X.; Thompson, G.E.; Nilsson, J.-O.; Gustavsson, M.; Crispin, A. Origin of Streaks on Anodised Aluminium Alloy Extrusions. *Trans. IMF* **2013**, *91*, 11–16. [[CrossRef](#)]
35. Bononi, M.; Giovanardi, R.; Bozza, A. Pulsed Current Hard Anodizing of Heat Treated Aluminum Alloys: Frequency and Current Amplitude Influence. *Surf. Coat. Technol.* **2016**, *307*, 861–870. [[CrossRef](#)]
36. Aggerbeck, M.; Canulescu, S.; Dirscherl, K.; Johansen, V.E.; Engberg, S.; Schou, J.; Ambat, R. Appearance of Anodised Aluminium: Effect of Alloy Composition and Prior Surface Finish. *Surf. Coat. Technol.* **2014**, *254*, 28–41. [[CrossRef](#)]
37. Wielage, B.; Nickel, D.; Alisch, G.; Podlesak, H.; Lampke, T. Effects of Pre-Treatment on the Growth Rate and Morphology of Hard Anodic Films on Aluminium (EN AW-6082). *Surf. Coat. Technol.* **2007**, *202*, 569–576. [[CrossRef](#)]
38. Gröber, D.; Georgi, W.; Sieber, M.; Scharf, L.; Hellmig, R.J.; Leidich, E.; Lampke, T.; Mayr, P. The Effect of Anodising on the Fatigue Performance of Self-Tapping Aluminium Screws. *Int. J. Fatigue* **2015**, *75*, 108–114. [[CrossRef](#)]
39. Stojadinović, S.; Vasilčić, R.; Petković, M.; Kasalica, B.; Belča, I.; Žekić, A.; Zeković, L. Characterization of the Plasma Electrolytic Oxidation of Titanium in Sodium Metasilicate. *Appl. Surf. Sci.* **2013**, *265*, 226–233. [[CrossRef](#)]
40. Lu, X.; Blawert, C.; Kainer, K.U.; Zheludkevich, M.L. Investigation of the Formation Mechanisms of Plasma Electrolytic Oxidation Coatings on Mg Alloy AM50 Using Particles. *Electrochim. Acta* **2016**, *196*, 680–691. [[CrossRef](#)]
41. Dehnavi, V.; Liu, X.Y.; Luan, B.L.; Shoesmith, D.W.; Rohani, S. Phase Transformation in Plasma Electrolytic Oxidation Coatings on 6061 Aluminum Alloy. *Surf. Coat. Technol.* **2014**, *251*, 106–114. [[CrossRef](#)]

42. Sobolev, A.; Kossenko, A.; Zinigrad, M.; Borodianskiy, K. An Investigation of Oxide Coating Synthesized on an Aluminum Alloy by Plasma Electrolytic Oxidation in Molten Salt. *Appl. Sci.* **2017**, *7*, 889. [CrossRef]
43. Sharma, A.; Jang, Y.-J.; Jung, J.P. Effect of KOH to Na<sub>2</sub>SiO<sub>3</sub> Ratio on Microstructure and Hardness of Plasma Electrolytic Oxidation Coatings on AA 6061 Alloy. *J. Mater. Eng. Perform.* **2017**, *26*, 5032–5042. [CrossRef]
44. Wang, K.; Koo, B.H.; Lee, C.G.; Kim, Y.J.; Lee, S.; Byon, E. Effects of Hybrid Voltages on Oxide Formation on 6061 Al-Alloys During Plasma Electrolytic Oxidation. *Chin. J. Aeronaut.* **2009**, *22*, 564–568. [CrossRef]
45. Zhu, Q.-J.; Wang, B.B.; Zhao, X.; Zhang, B.B. Robust Micro Arc Oxidation Coatings on 6061 Aluminum Alloys via Surface Thickening and Microvoid Reducing Approach. In *Metallurgy Technology and Materials VI, Proceedings of the 6th International Conference on Metallurgy Technology and Materials, Xi'an, China, May 30–31 2018*; Trans Tech Publications Ltd.: Baech, Switzerland, 2018; Volume 279, pp. 148–152.
46. Sowa, M.; Wala, M.; Blacha-Grzechnik, A.; Maciej, A.; Kazek-Kęsik, A.; Stolarczyk, A.; Simka, W. Corrosion Inhibitor-Modified Plasma Electrolytic Oxidation Coatings on 6061 Aluminum Alloy. *Materials* **2021**, *14*, 619. [CrossRef] [PubMed]
47. Ma, K.-J.; Al Bosta, M.M.S.; Wu, W.-T. Preparation of Self-Lubricating Composite Coatings through a Micro-Arc Plasma Oxidation with Graphite in Electrolyte Solution. *Surf. Coat. Technol.* **2014**, *259*, 318–324. [CrossRef]
48. Chen, Q.; Jiang, Z.; Tang, S.; Dong, W.; Tong, Q.; Li, W. Influence of Graphene Particles on the Micro-Arc Oxidation Behaviors of 6063 Aluminum Alloy and the Coating Properties. *Appl. Surf. Sci.* **2017**, *423*, 939–950. [CrossRef]
49. Jiang, D.; Xia, X.; Hou, J.; Zhang, X.; Dong, Z. Enhanced Corrosion Barrier of Microarc-Oxidized Mg Alloy by Self-Healing Superhydrophobic Silica Coating. *Ind. Eng. Chem. Res.* **2019**, *58*, 165–178. [CrossRef]
50. Martin, J.; Nominé, A.; Ntomprougkidis, V.; Migot, S.; Bruyère, S.; Soldera, F.; Belmonte, T.; Henrion, G. Formation of a Metastable Nanostructured Mullite during Plasma Electrolytic Oxidation of Aluminium in “Soft” Regime Condition. *Mater. Des.* **2019**, *180*, 107977. [CrossRef]
51. Clyne, T.W.; Troughton, S.C. A Review of Recent Work on Discharge Characteristics during Plasma Electrolytic Oxidation of Various Metals. *Int. Mater. Rev.* **2019**, *64*, 127–162. [CrossRef]
52. Matykina, E.; Arrabal, R.; Mohedano, M.; Mingo, B.; Gonzalez, J.; Pardo, A.; Merino, M.C. Recent Advances in Energy Efficient PEO Processing of Aluminium Alloys. *Trans. Nonferrous Met. Soc. China* **2017**, *27*, 1439–1454. [CrossRef]
53. Hong, L.; Wang, D.; Bian, G.-D.; Wang, L.-L.; Hu, S.-G. Self-Lubricating PEO Coating on an Al Alloy Produced by Vacuum Impregnation Post-Treatment. *Acta Metall. Sin. (Engl. Lett.)* **2015**, *28*, 965–974. [CrossRef]
54. Al Bosta, M.M.S.; Ma, K.-J. Suggested Mechanism for the MAO Ceramic Coating on Aluminium Substrates Using Bipolar Current Mode in the Alkaline Silicate Electrolytes. *Appl. Surf. Sci.* **2014**, *308*, 121–138. [CrossRef]
55. Walsh, F.C.; Low, C.T.J.; Wood, R.J.K.; Stevens, K.T.; Archer, J.; Poeton, A.R.; Ryder, A. Plasma Electrolytic Oxidation (PEO) for Production of Anodised Coatings on Lightweight Metal (Al, Mg, Ti) Alloys. *Trans. IMF* **2009**, *87*, 122–135. [CrossRef]
56. Simchen, F.; Sieber, M.; Kopp, A.; Lampke, T. Introduction to Plasma Electrolytic Oxidation—An Overview of the Process and Applications. *Coatings* **2020**, *10*, 628. [CrossRef]
57. Tran, Q.P. Plasma Electrolytic Oxidation Coating On 6061 Al Alloy Using An Electrolyte Without Alkali Ions. *Vietnam J. Sci. Technol.* **2018**, *54*, 151. [CrossRef]
58. Chen, Y.; Song, X.; Zhou, J.; Liu, H.; Yang, Y. The Study on the Overall Plasma Electrolytic Oxidation for 6061–7075 Dissimilar Aluminum Alloy Welded Parts Based on the Dielectric Breakdown Theory. *Materials* **2018**, *11*, 63. [CrossRef] [PubMed]
59. Treviño, M.; Garza-Montes-de-Oca, N.F.; Pérez, A.; Hernández-Rodríguez, M.A.L.; Juárez, A.; Colás, R. Wear of an Aluminium Alloy Coated by Plasma Electrolytic Oxidation. *Surf. Coat. Technol.* **2012**, *206*, 2213–2219. [CrossRef]
60. Peng, Z.; Xu, H.; Liu, S.; Qi, Y.; Liang, J. Wear and Corrosion Resistance of Plasma Electrolytic Oxidation Coatings on 6061 Al Alloy in Electrolytes with Aluminate and Phosphate. *Materials* **2021**, *14*, 4037. [CrossRef] [PubMed]
61. Tran, Q.-P.; Chin, T.-S.; Kuo, Y.-C.; Jin, C.-X.; Trung, T.; Tuan, C.V.; Dang, D.Q. Diamond Powder Incorporated Oxide Layers Formed on 6061 Al Alloy by Plasma Electrolytic Oxidation. *J. Alloys Compd.* **2018**, *751*, 289–298. [CrossRef]
62. Byeon, S.S.; Wang, K.; Jung, Y.G.; Koo, B.H. Characteristic of AlON–Al<sub>2</sub>O<sub>3</sub> Coatings on Al6061 Alloy by Electrolytic Plasma Processing in Aluminate and Nitride Electrolytes. *Surf. Coat. Technol.* **2010**, *204*, 3196–3199. [CrossRef]
63. Madhavi, Y.; Narasaiah, N.; Jyothirmayi, A.; Rama Krishna, L. Influence of Surface-Roughness on the Corrosion-Fatigue Behavior of MAO Coated 6061-T6 Al Alloy Assessed in NaCl Medium. *Surf. Coat. Technol.* **2021**, *414*, 127102. [CrossRef]
64. Zhang, Y.; Fan, W.; Du, H.Q.; Zhao, Y.W. Corrosion Behavior and Structure of Plasma Electrolytic Oxidation Coated Aluminum Alloy. *Int. J. Electrochem. Sci.* **2017**, *12*, 6788–6800. [CrossRef]
65. Malayoglu, U.; Tekin, K.C.; Malayoglu, U.; Shrestha, S. An Investigation into the Mechanical and Tribological Properties of Plasma Electrolytic Oxidation and Hard-Anodized Coatings on 6082 Aluminum Alloy. *Mater. Sci. Eng. A* **2011**, *528*, 7451–7460. [CrossRef]
66. Shrestha, S.; Dunn, B.D. Plasma electrolytic oxidation and anodising of aluminium alloys for spacecraft applications. In *Surface Engineering of Light Alloys*; Woodhead Publishing: Sawston, UK, 2010. Available online: <https://www.sciencedirect.com/science/article/pii/B978184569537850018X?via%3Dihub> (accessed on 2 January 2022).
67. Yürektürk, Y.; Muhaffel, F.; Baydoğan, M. Characterization of Micro Arc Oxidized 6082 Aluminum Alloy in an Electrolyte Containing Carbon Nanotubes. *Surf. Coat. Technol.* **2015**, *269*, 83–90. [CrossRef]
68. Yan, H.; Wang, J.; Meng, C.; Wang, X.; Song, S.; Fan, X.; Zhang, L.; Li, H.; Li, W.; Zhu, M. Towards Long-Term Corrosion and Wear Protection of Al Alloy: Synergy of Ti<sub>3</sub>C<sub>2</sub>T<sub>x</sub> Flake and Micro-Arc Oxidation Coating. *Corros. Sci.* **2020**, *174*, 108813. [CrossRef]

69. Ralls, A.M.; Kasar, A.K.; Menezes, P.L. Friction Stir Processing on the Tribological, Corrosion, and Erosion Properties of Steel: A Review. *J. Manuf. Mater. Process.* **2021**, *5*, 97. [[CrossRef](#)]
70. Kumar Rajak, D.; Pagar, D.D.; Menezes, P.L.; Eyvazian, A. Friction-Based Welding Processes: Friction Welding and Friction Stir Welding. *J. Adhes. Sci. Technol.* **2020**, *34*, 2613–2637. [[CrossRef](#)]
71. Kurt, A.; Uygur, I.; Cete, E. Surface Modification of Aluminium by Friction Stir Processing. *J. Mater. Process. Technol.* **2011**, *211*, 313–317. [[CrossRef](#)]
72. Rathee, S.; Maheshwari, S.; Siddiquee, A.N.; Srivastava, M. A Review of Recent Progress in Solid State Fabrication of Composites and Functionally Graded Systems Via Friction Stir Processing. *Crit. Rev. Solid State Mater. Sci.* **2018**, *43*, 334–366. [[CrossRef](#)]
73. Girish, G.; Anandakrishnan, V. A Study on the Microstructure, Hardness, and Tribological Behavior of Aluminum-Based Metal–Matrix Composite Fabricated through Recursive Friction Stir Processing. *Proc. Inst. Mech. Eng. Part L J. Mater. Des. Appl.* **2021**, *235*, 671–683. [[CrossRef](#)]
74. Singh, P.; Kandikonda, H.R. Friction Stir Processing of Aluminum Alloys. *Indian J. Eng. Mater. Sci.* **2021**, *28*, 16.
75. Mehta, K.M.; Badheka, V.J. Effect of Friction Stir Processing Passes on Wear Properties of Al-6061-T6 Alloy. *J. Braz. Soc. Mech. Sci. Eng.* **2021**, *43*, 199. [[CrossRef](#)]
76. Zhao, H.; Pan, Q.; Qin, Q.; Wu, Y.; Su, X. Effect of the Processing Parameters of Friction Stir Processing on the Microstructure and Mechanical Properties of 6063 Aluminum Alloy. *Mater. Sci. Eng. A* **2019**, *751*, 70–79. [[CrossRef](#)]
77. Patel, V.V.; Badheka, V.; Kumar, A. Friction Stir Processing as a Novel Technique to Achieve Superplasticity in Aluminum Alloys: Process Variables, Variants, and Applications. *Metallogr. Microstruct. Anal.* **2016**, *5*, 278–293. [[CrossRef](#)]
78. Shafiei Zarghani, A.; Kashani Bozorg, S.F.; Zarei-Hanzaki, A. Ultrafine Grained 6082 Aluminum Alloy Fabricated by Friction Stir Processing. *Int. J. Mod. Phys. B* **2008**, *22*, 2874–2878. [[CrossRef](#)]
79. Kumar, S. Ultrasonic Assisted Friction Stir Processing of 6063 Aluminum Alloy. *Arch. Civ. Mech. Eng.* **2016**, *16*, 473–484. [[CrossRef](#)]
80. Senthilkumar, R.; Prakash, M.; Arun, N.; Jeyakumar, A.A. The Effect of the Number of Passes in Friction Stir Processing of Aluminum Alloy (AA6082) and Its Failure Analysis. *Appl. Surf. Sci.* **2019**, *491*, 420–431. [[CrossRef](#)]
81. Al-Fadhalah, K.; Asi, F. Aging Behavior of Aluminum Alloy 6082 Subjected to Friction Stir Processing. *Crystals* **2018**, *8*, 337. [[CrossRef](#)]
82. Sarvaiya, J.; Singh, D. Determination of defect-free working range of friction stir processing for AA6082-T6. In *Recent Advances in Smart Manufacturing and Materials, Proceedings of the International Conference on Evolution in Manufacturing (ICEM 2020), Online, 10–12 December 2020*; Agrawal, R., Jain, J.K., Yadav, V.S., Manupati, V.K., Varela, L., Eds.; Springer: Singapore, 2021; pp. 327–339.
83. Mane, K.M.; Hosmani, S.S. Friction Stir Surface Processing of Al 6061 Alloy: Role of Surface Alloying with Copper and Heat-Treatment. *Trans. Indian Inst. Met.* **2018**, *71*, 1411–1425. [[CrossRef](#)]
84. Balakrishnan, M.; Dinaharan, I.; Palanivel, R.; Sathiskumar, R. Effect of Friction Stir Processing on Microstructure and Tensile Behavior of AA6061/Al3Fe Cast Aluminum Matrix Composites. *J. Alloys Compd.* **2019**, *785*, 531–541. [[CrossRef](#)]
85. Miranda, R.M.; Gandra, J.; Vilaça, P. Surface modification by friction based processes. In *Modern Surface Engineering Treatments*; IntechOpen: London, UK, 2013; ISBN 978-953-51-1149-8.
86. Choi, D.-H.; Kim, Y.-I.; Kim, D.-U.; Jung, S.-B. Effect of SiC Particles on Microstructure and Mechanical Property of Friction Stir Processed AA6061-T4. *Trans. Nonferrous Met. Soc. China* **2012**, *22*, s614–s618. [[CrossRef](#)]
87. Eftekharinia, H.; Amadeh, A.A.; Khodabandeh, A.; Paidar, M. Microstructure and Wear Behavior of AA6061/SiC Surface Composite Fabricated via Friction Stir Processing with Different Pins and Passes. *Rare Met.* **2020**, *39*, 429–435. [[CrossRef](#)]
88. Salehi, M.; Saadatmand, M.; Aghazadeh Mohandesi, J. Optimization of Process Parameters for Producing AA6061/SiC Nanocomposites by Friction Stir Processing. *Trans. Nonferrous Met. Soc. China* **2012**, *22*, 1055–1063. [[CrossRef](#)]
89. Mehdi, H.; Mishra, R.S. Effect of Multi-Pass Friction Stir Processing and SiC Nanoparticles on Microstructure and Mechanical Properties of AA6082-T6. *Adv. Ind. Manuf. Eng.* **2021**, *3*, 100062. [[CrossRef](#)]
90. Salehi, M.; Farnoush, H.; Mohandesi, J.A. Fabrication and Characterization of Functionally Graded Al–SiC Nanocomposite by Using a Novel Multistep Friction Stir Processing. *Mater. Des.* **2014**, *63*, 419–426. [[CrossRef](#)]
91. Zuhailawati, H.; Halmy, M.N.; Almanar, I.P.; Dhindaw, B.K. Friction Stir Processed of 6061-T6 Aluminum Alloy Reinforced with Silica from Rice Husk Ash. *Adv. Mater. Res.* **2014**, *1024*, 227–230. [[CrossRef](#)]
92. Mazaheri, Y.; Heidarpour, A.; Jalilvand, M.M.; Roknian, M. Effect of Friction Stir Processing on the Microhardness, Wear and Corrosion Behavior of Al6061 and Al6061/SiO<sub>2</sub> Nanocomposites. *J. Mater. Eng. Perform.* **2019**, *28*, 4826–4837. [[CrossRef](#)]
93. Devaraju, A.; Kumar, A.; Kumaraswamy, A.; Kotiveerachari, B. Influence of Reinforcements (SiC and Al<sub>2</sub>O<sub>3</sub>) and Rotational Speed on Wear and Mechanical Properties of Aluminum Alloy 6061-T6 Based Surface Hybrid Composites Produced via Friction Stir Processing. *Mater. Des.* **2013**, *51*, 331–341. [[CrossRef](#)]
94. Qu, J.; Xu, H.; Feng, Z.; Frederick, D.A.; An, L.; Heinrich, H. Improving the Tribological Characteristics of Aluminum 6061 Alloy by Surface Compositing with Sub-Micro-Size Ceramic Particles via Friction Stir Processing. *Wear* **2011**, *271*, 1940–1945. [[CrossRef](#)]
95. Naresh, P.; Kumar, A.; Krishna Kishore, M. Influence of Nano Reinforcement Volume Percentage on Fabrication of Surface Nanocomposite by FSP. *Mater. Sci. Forum* **2017**, *879*, 1369–1374. [[CrossRef](#)]
96. Guo, J.F.; Liu, J.; Sun, C.N.; Maleksaedi, S.; Bi, G.; Tan, M.J.; Wei, J. Effects of Nano-Al<sub>2</sub>O<sub>3</sub> Particle Addition on Grain Structure Evolution and Mechanical Behaviour of Friction-Stir-Processed Al. *Mater. Sci. Eng. A* **2014**, *602*, 143–149. [[CrossRef](#)]

97. Kheirkhah, S.; Imani, M.; Aliramezani, R.; Zamani, M.H.; Kheilnejad, A. Microstructure, Mechanical Properties and Corrosion Resistance of Al6061/BN Surface Composite Prepared by Friction Stir Processing. *Surf. Topogr. Metrol. Prop.* **2019**, *7*, 035002. [[CrossRef](#)]
98. Patel, S.K.; Singh, V.P.; Kuriachen, B. Modification of Aluminium Alloy Surface Composite Reinforced with ZrO<sub>2</sub> Particles Fabricated Through Friction Stir Processing. In *Advances in Additive Manufacturing and Joining, Proceedings of the 7th International and 28th All India Manufacturing Technology, Design and Research conference, Chennai, India, 13–15 December 2018*; Shunmugam, M.S., Kanthababu, M., Eds.; Springer: Singapore, 2020; pp. 579–586.
99. Rathee, S.; Maheshwari, S.; Siddiquee, A.N.; Srivastava, M. Distribution of Reinforcement Particles in Surface Composite Fabrication via Friction Stir Processing: Suitable Strategy. *Mater. Manuf. Process.* **2018**, *33*, 262–269. [[CrossRef](#)]
100. Palanivel, R.; Dinaharan, I.; Laubscher, R.F.; Davim, J.P. Influence of Boron Nitride Nanoparticles on Microstructure and Wear Behavior of AA6082/TiB<sub>2</sub> Hybrid Aluminum Composites Synthesized by Friction Stir Processing. *Mater. Des.* **2016**, *106*, 195–204. [[CrossRef](#)]
101. Vatankhah Barenji, R.; Khojastehnezhad, V.M.; Pourasl, H.H.; Rabieezadeh, A. Wear Properties of Al–Al<sub>2</sub>O<sub>3</sub>/TiB<sub>2</sub> Surface Hybrid Composite Layer Prepared by Friction Stir Process. *J. Compos. Mater.* **2016**, *50*, 1457–1466. [[CrossRef](#)]
102. Anvari, S.R.; Karimzadeh, F.; Enayati, M.H. Wear Characteristics of Al–Cr–O Surface Nano-Composite Layer Fabricated on Al6061 Plate by Friction Stir Processing. *Wear* **2013**, *304*, 144–151. [[CrossRef](#)]
103. Anandha Kumar, C.J.; Gopi, S.; Kumar, S.S.; Mohan, D.G. Mechanical, Metallurgical and Tribological Properties of Friction Stir Processed Aluminium Alloy 6061 Hybrid Surface Composites. *Surf. Topogr. Metrol. Prop.* **2021**, *9*, 045019. [[CrossRef](#)]
104. Dinesh, D.; Megalingam, A.; Rajamurugan, G.; Arundeeep, M.; Tajdeen, A. Wear and Microstructure Characteristics of Friction Stir Processed Al6063/B<sub>4</sub>C+SiO<sub>2</sub> Composites. *Adv. Asp. Eng. Res.* **2021**, *3*, 140–150. [[CrossRef](#)]
105. Bararpour, S.M.; Aval, H.J.; Jamaati, R. An Experimental and Theoretical Investigation of Thermo-Mechanical Issues in Friction Surfacing of Al-Mg Aluminium Alloys: Material Flow and Residual Stress. Modelling Simul. *Mater. Sci. Eng.* **2020**, *28*, 035003. [[CrossRef](#)]
106. Jujare, T.; Kumar, A.; Kailas, S.V.; Bhat, K.U. Friction Surfacing of Mild Steel by Copper: A Feasibility Study. *Procedia Mater. Sci.* **2014**, *5*, 1300–1307. [[CrossRef](#)]
107. Gandra, J.; Miranda, R.M.; Vilaça, P. Performance Analysis of Friction Surfacing. *J. Mater. Process. Technol.* **2012**, *212*, 1676–1686. [[CrossRef](#)]
108. Kallien, Z.; Rath, L.; Roos, A.; Klusemann, B. Experimentally Established Correlation of Friction Surfacing Process Temperature and Deposit Geometry. *Surf. Coat. Technol.* **2020**, *397*, 126040. [[CrossRef](#)]
109. Ehrich, J.; Roos, A.; Hanke, S. Effect of Mg and Si content in aluminum alloys on friction surfacing processing behavior. In *Light Metals 2019, Proceedings of the TMS 2019 Annual Meeting and Exhibition, San Antonio, TX, USA, 10–14 March 2019*; Chesonis, C., Ed.; Springer: Cham, Switzerland, 2019; pp. 357–363.
110. Krohn, H.; Hanke, S.; Beyrer, M.; dos Santos, J.F. Influence of External Cooling Configuration on Friction Surfacing of AA6082 T6 over AA2024 T351. *Manuf. Lett.* **2015**, *5*, 17–20. [[CrossRef](#)]
111. Gandra, J.; Pereira, D.; Miranda, R.M.; Silva, R.J.C.; Vilaça, P. Deposition of AA6082-T6 over AA2024-T3 by Friction Surfacing—Mechanical and Wear Characterization. *Surf. Coat. Technol.* **2013**, *223*, 32–40. [[CrossRef](#)]
112. Gandra, J.; Vigarinho, P.; Pereira, D.; Miranda, R.M.; Velinho, A.; Vilaça, P. Wear Characterization of Functionally Graded Al–SiC Composite Coatings Produced by Friction Surfacing. *Mater. Des.* **2013**, *52*, 373–383. [[CrossRef](#)]
113. Vijaya Kumar, B.; Madhusudhan Reddy, G.; Mohandas, T. Identification of Suitable Process Parameters for Friction Surfacing of Mild Steel with AA6063 Aluminium Alloy. *Int. J. Adv. Manuf. Technol.* **2014**, *74*, 433–443. [[CrossRef](#)]
114. Yuvaraj, N. Improving the Wear Properties of Aluminum 6082 Alloy by Surface Compositing with ZrO<sub>2</sub> Ceramic Particles Via Friction Stir Processing. *Mater. Sci. Res. India* **2018**, *15*, 68–74. [[CrossRef](#)]
115. John, M.; Kalvala, P.R.; Misra, M.; Menezes, P.L. Peening Techniques for Surface Modification: Processes, Properties, and Applications. *Materials* **2021**, *14*, 3841. [[CrossRef](#)] [[PubMed](#)]
116. Zhu, L.; Xue, P.; Lan, Q.; Meng, G.; Ren, Y.; Yang, Z.; Xu, P.; Liu, Z. Recent Research and Development Status of Laser Cladding: A Review. *Opt. Laser Technol.* **2021**, *138*, 106915. [[CrossRef](#)]
117. Zhou, J.; Han, X.; Li, H.; Liu, S.; Yi, J. Investigation of Layer-by-Layer Laser Remelting to Improve Surface Quality, Microstructure, and Mechanical Properties of Laser Powder Bed Fused AlSi<sub>10</sub>Mg Alloy. *Mater. Des.* **2021**, *210*, 110092. [[CrossRef](#)]
118. de Oliveira, U.; Ocelík, V.; De Hosson, J.T.M. Analysis of Coaxial Laser Cladding Processing Conditions. *Surf. Coat. Technol.* **2005**, *197*, 127–136. [[CrossRef](#)]
119. Henri, P.; Jonne, N.; Sebastian, T.; Jari, T.; Steffen, N.; Petri, V. Laser cladding with coaxial wire feeding. In *Proceedings of the International Congress on Applications of Lasers & Electro Optics (ICALEO), Anaheim, CA, USA, 23–27 September 2012*; pp. 1196–1201. [[CrossRef](#)]
120. Wirth, F.; Wegener, K. A Physical Modeling and Predictive Simulation of the Laser Cladding Process. *Addit. Manuf.* **2018**, *22*, 307–319. [[CrossRef](#)]
121. Vilar, R. Laser Cladding. *J. Laser Appl.* **1999**, *11*, 64–79. [[CrossRef](#)]
122. Li, M.; Han, B.; Song, L.; He, Q. Enhanced Surface Layers by Laser Cladding and Ion Sulfurization Processing towards Improved Wear-Resistance and Self-Lubrication Performances. *Appl. Surf. Sci.* **2020**, *503*, 144226. [[CrossRef](#)]

123. Farahmand, P.; Liu, S.; Zhang, Z.; Kovacevic, R. Laser Cladding Assisted by Induction Heating of Ni–WC Composite Enhanced by Nano-WC and La<sub>2</sub>O<sub>3</sub>. *Ceram. Int.* **2014**, *40*, 15421–15438. [[CrossRef](#)]
124. Zarezadeh Mehrizi, M.; Shamanian, M.; Saidi, A.; Shoja-Razazvi, R.; Beigi, R. Evaluation of Oxidation Behavior of Laser Clad CoWSi–WSi<sub>2</sub> Coating on Pure Ni Substrate at Different Temperatures. *Ceram. Int.* **2015**, *41*, 9715–9721. [[CrossRef](#)]
125. Wang, C.; Gao, Y.; Wang, R.; Wei, D.; Cai, M.; Fu, Y. Microstructure of Laser-Clad Ni60 Cladding Layers Added with Different Amounts of Rare-Earth Oxides on 6063 Al Alloys. *J. Alloys Compd.* **2018**, *740*, 1099–1107. [[CrossRef](#)]
126. Wang, C.; Gao, Y.; Zeng, Z.; Fu, Y. Effect of Rare-Earth on Friction and Wear Properties of Laser Cladding Ni-Based Coatings on 6063Al. *J. Alloys Compd.* **2017**, *727*, 278–285. [[CrossRef](#)]
127. Menezes, P.L.; Nosonovsky, M.; Kailas, S.V.; Lovell, M.R. Friction and wear. In *Tribology for Scientists and Engineers: From Basics to Advanced Concepts*; Menezes, P.L., Nosonovsky, M., Ingole, S.P., Kailas, S.V., Lovell, M.R., Eds.; Springer: New York, NY, USA, 2013; pp. 43–91, ISBN 978-1-4614-1945-7.